Marine Geophysical Research (2021) 42:35
https://doi.org/10.1007/s11001-021-09458-6

ORIGINAL RESEARCH PAPER

Proposing a new strategy in multi-seismic attribute combination for identification of buried channel

Hassan Khasraji-Nejad[1] · Amin Roshandel Kahoo[2] · Mehrdad Soleimani Monfared[2,3] · Mohammad Radad[2] · Keyvan Khayer[2]

Received: 21 February 2021 / Accepted: 17 October 2021

Abstract

The seismic data interpretation reveals properties of the subsurface structures, appropriate for further geological or exploration investigations. The buried channels are desired exploratory targets for petroleum reservoir exploration, drilling concerns or geological investigations. Therefore, it is required to precisely identify the geometry of the buried channels through the signal image analysis and the geological interpretation of the seismic data. The continuous wavelet transform (CWT) is a spectral discrete transform method for non-stationary signal analysis, useful to enhance the resolution of the seismic data both in time and frequency domains. In the presented study, we propose a strategy for a precise identification of buried channels, using a vast number of time–frequency seismic attributes on 3D seismic data. The spectral decomposition by the CWT method has been performed on 20, 25, 30, 35, and 40 Hz frequency sections. The seismic attributes have been extracted, including the energy, the instantaneous amplitude, the average root mean square, the Prewitt and Grubbs filters, the similarity, the semblance, and the grey-level covariance matrix. The most favorable results have been selected to be integrated, so providing new attributes through RGB composition. This integration has been performed both for single frequency and multi-frequency seismic sections. As a result of applying the proposed strategy on the selected synthetic and field dataset, the boundaries of the buried channel as well as its inner structure, have been individuated. The final model of the seismic attributes has revealed that the proposed strategy represents an alternative to the conventional procedure of identification the buried channel.

Keywords Seismic attribute · RGB composition · CWT · Attribute combination · Buried channel

Introduction

Application of seismic attributes in the geological interpretation is not a new task, due to the increasing number of attributes and their wide majority of applications, it is a complicated task to select and apply the most relevant attributes to extract the required information (Bulat and Long 2001; Damuth and Olson 2001). There are various types of geological objects as the target of investigation through seismic data processing and interpretation, that require an appropriate use of seismic attributes in a comprehensive integration strategy (Civile et al. 2014; Farfour et al. 2015; Hsiung et al. 2015). A vast number of seismic attributes besides the time-consuming procedure of geological interpretation on especially large 3D seismic data, emphasizes the introduction of integration methods for accurate interpretation. Although it is near than a decade that several imaging tools such as group of pattern recognition methods are frequently used in

✉ Amin Roshandel Kahoo
roshandel@shahroodut.ac.ir

Hassan Khasraji-Nejad
h.khasreji72@shahroodut.ac.ir

Mehrdad Soleimani Monfared
msoleimani@shahroodut.ac.ir;
mehrdad.soleimani@partner.kit.edu

Mohammad Radad
mradad@shahroodut.ac.ir

Keyvan Khayer
k.khayer@shahroodut.ac.ir

[1] Master Educated of Exploration Seismology, Shahrood University of Technology, Shahrood, Iran

[2] Faculty of Mining, Petroleum and Geophysics Engineering, Shahrood University of Technology, Shahrood, Iran

[3] Geophysical Institute (GPI), Karlsruhe Institute of Technology (KIT), Karlsruhe, Germany

Published online: 02 November 2021

seismic interpretation, however, we still need to look for a strategy that combines several information layers obtained from attributes to identify the geological object in the seismic data with less uncertainty. These objects are commonly mud/shale diapirs, salt dome, the gas chimney and the buried channels (Bourget et al. 2014; Radad et al. 2015; Soleimani 2015; Tvedt et al. 2016). Raef et al. (2016) stated that combination of various seismic attributes provides a final integrated model that better identity the target under investigation, like as the buried channel, compared when analyzing with single attribute. Detection and modeling the buried channel system by seismic attributes conventionally consist of two steps. The first step is the selection of attributes enhancing any difference in the characteristics of the buried channel regarding its seismic pattern, while the second step is the identification of its boundary (Iacopini et al. 2016; Auguy et al. 2017).

Considering identification of the buried channel, the geological type of the channel system should be identified. Kolla et al. (2007) comprehensively investigated and compared properties of the fluvial sinuous channel and the deep-water canyons related channels. They have stated that the point-bar scrolls, cutoffs, downstream sweeps of channel bends and sinusitis can be found in seismic time slices. They also have shown that the point-bar scrolls in a fluvial system can be identified by high seismic-amplitude and high channel sinuosity. Deep-water sinuous channel complexes, however, have some properties in common with the fluvial channels, and differ in other properties. Generally, a large valley hosts the complexes of the sinuous channel and its related banks, flanked by large overbanks. In such a complex system, the top portions of sinuous channel growth may extend beyond the confines of the master valley and overlie the master overbanks. In the seismic time slices related to this type of the channels, high-amplitude with multiple sinuous threads or multiple sinuous bands (Kolla et al. 2007). Considering development of the channel system in the submarine canyon formation, slope failure is a characteristic trigger process for the developing system of the submarine canyons, when an adequate mass source like delta facies sediments are available (Hui et al. 2018). Lomask et al. (2007) introduced a methodology for integration of the seismic attributes to identify the boundaries of geological object in seismic images based on the image-segmentation concept. They have presented a modification of the normalized cuts image segmentation for tracking object boundaries in the seismic image. They have mentioned that the amplitude alone may not fully define the boundaries, thus incorporated any number of attributes to fully exploit the dimensionality of the data. To obtain better result, they used a weighting operator to weight each attribute. The weights are determined using problem-dependent combinations of attributes. Nevertheless, the boundaries of the geological objects by the seismic data should be defined as accurate as possible. Thus any further geological interpretation or drilling path determination on seismic images with the unclear boundaries of geological objects is uncertain (Berthelot et al. 2011). Berthelot et al. (2013) proposed a strategy by the combination of numerous attributes to improve the accuracy of interpretation on the integrated image. They have combined the frequency-based attributes with, the similarity, the dip and the grey-level-co-occurrence matrix (GLCM). This combination was followed by a supervised Bayesian classification's method. Chuai et al. (2014) have presented a seismic texture coherence algorithm efficient for channel detection in seismic data. They have analyzed the texture feature parameters in different azimuths in 3D seismic data. Based on variation of feature parameters in different angles, they have introduced the seismic texture attribute. Their selected feature parameters were an average of the amplitude, the dissimilarity, the entropy, the variance, the second moment angular and the inverse difference moment. These parameters have shown that the difference between the sand filled channel system and the enclosing medium, composed of mudstones, was exaggerated in the seismic texture coherence attribute image, and thus the channel system could be clearly imaged. Halpert et al. (2014) stated that incorporation of the interpreter decision on the seismic attribute interpretation reduces the uncertainty of the detection of the geological object in areas with a less clear boundary. This strategy is effective in seismic data with strong contrast of amplitude in the object boundaries. It will also reduce the risk of wrong interpretation by interpreter interaction in low amplitudes segments. However, their proposed methodology is a time consuming and challenging method for large 3D seismic data, while it also suffers from low information in problematic areas for 2D data. Amin and Deriche (2015b) introduced a robust method for object detection in 2D seismic data by a combination of edge and texture attributes to overcome the problems of texture attributes that depends on the nature of geological object under investigation. Wang et al. (2015) introduced a boundary detection algorithm based on the texture attributes using tensor and subspace learning. Their method consists of two steps in boundary detection by the texture-based gradient followed by a tensor-based subspace learning process. This method could provide an efficient and robust practical labeling tool for high quality data. However, in data with a less clear or gradual boundary, this method might fail due to lower contrast between adjacent seismic events. Campbell et al. (2015) have shown that integration of the well data with the acoustic impedance and the reflection amplitude can enhance geological interpretation on the deep see canyon related channel in the Penobscot 3D seismic data. They have shown that their method could improve geological interpretation on the sandstones reservoirs with low impedance, presented in the extensive unconstrained

marginal marine systems and also in the complex confined channel systems. They also could identify and separate the carbonate bank with high impedance, interfingering with low impedance shales. Amin and Deriche (2016) developed the strategy of Amin and Deriche (2015a) by introducing the GLCM to the former method. The algorithm of Amin and Deriche (2016) combines the attributes from the GLCM and those from the Gabor filter, with a codebook-based learning approach to delineate the object boundaries in seismic image attributes. However, this method still needs an interpreter interaction in the last stage in refining the final boundary using edge strength values. Wu (2016) introduced a method to calculate the likelihoods of seismic events in attribute images to define the boundary of the object. Wu (2016) mentioned that the second step in their method, which is using attributes to extract the boundaries is important for computing boundaries, especially when the input data are noisy or incomplete. They have proposed that any attributes can also be used for boundary extraction. Manually interpreted points, segments or surface patches can be used as constraints to compute a more reliable and reasonable boundaries. However, the method is still computationally expensive and requires excess effort and accuracy in the first step on constructing the structure tensor field. Li et al. (2016) presented multi-seismic attributes analysis to define the distributary channels in 3D seismic data. They have compared result of the short time Fourier transform (STFT) and the continuous wavelet transform (CWT) methods to extract the 40 Hz single frequency image and stated that the CWT method provides attribute image with higher quality and better identification of the channel compared to using the STFT method. Therefore, they have used the CWT method for spectral decomposition and presented an enhanced image of the channel in seismic data by integration of 40 Hz single frequency attribute and the root mean square (RMS) attribute. Mirkamali et al. (2016) have used a combination of numerous attributes for the channel detection in 3D seismic data and used the artificial neural network (ANN) to define the weight of each attribute for combination. They have used the similarity, the dip, the curvature and the spectral decomposition attributes for identification of the buried channel. They have shown the single frequency map of 25 Hz, which was obtained by the STFT method was helpful in the separation of the channel system from their surrounding media. All the mentioned attribute combination for an accurate identification of the channel system in 3D seismic data have used only an ordinary combination of seismic attributes to provide an integrated image, without concerning the importance of information hiding in each single attribute. Shafiq et al. (2017) introduced a texture-based interpretation strategy to define the geological object on seismic attribute images. Their methodology was mapping an attribute called 3D gradient of texture (3D-GoT) to measure dissimilarity between voxel of data in all direction. This methodology was a stepwise workflow that selects the voxels related to the object by a tensor-based automatic seed point selection method.

In this study, we propose a strategy on the combination of the seismic attributes related to the channel detection on three-dimensional seismic data, according to the importance of information in each single attribute, which can be used for a better detection of the channel system. In the following, the proposed strategy would be explained in detail and the information and concept of each related attributes would be explained in the subsequent section. The methodology would be applied on a synthetic and field 3D seismic data containing a distributary channel system, where its minor branches could not be revealed by conventional attribute or seismic-multi attribute analysis.

The proposed strategy

The methodology herein proposed is based on the strategies that were used by Li et al. (2016) and Mirkamali et al. (2016). Their strategy was developed here by performing a wide analysis on seismic attributes and a combination of more seismic attributes, rather than simple combination of two seismic attributes. The proposed methodology aims to find a strategy in the combination of multi-seismic attributes attaining a unique model exhibiting the buried channel system in 3D seismic data. The research was initiated by performing a wide study of the existing literature on seismic attributes for enhancing the buried channels. The literature study consists of an investigation of the seismic attributes for the channel system detection and in the definition of the relative importance of each attribute in enhancing channel system and identifying the most suitable seismic attribute in imaging the boundary of the channel, separating the buried channel from the enclosing medium. Table 1 shows used seismic attributes used in the literature for the detection of the channel systems in seismic data. Table 1 is based on the explanatory function and and the target function. The exploratory function is generally used for an implicit definition of the object boundary (here's the channel boundary), which could be applied for primary interpretation. The target function is used for an explicit delineation of the geological body (the channel body here), in more detailed geological modeling and interpretation. The relative importance of the seismic attributes was defined based on the methodology introduced by Farrokhnia et al. (2018). These authors have presented a methodology in order to define the relative importance of the seismic attributes in predicting the salt body in attribute images. We have used the same concepts but for predicting the channel systems in 3D seismic data, from seismic attributes. After selecting the most relative attributes related to the detection of the channel system, a strategy was defined for an efficient combination of

Table 1 Target and explanatory functions used for buried channel detection by seismic attributes

Geoscience fields	Target function	Explanatory function
Seismic parameters in channel detection		
Low amplitude	+ +	+ + + +
Medium coherency	+ + + +	+ + + +
Low acoustic impedance	+ + + +	+ + + +
Low signal to noise ratio	+ + +	+ + +
Chaotic pattern	+ + + + +	+ + + + +
High similarity	+ + + +	+ + + + +
Low energy	+ + + +	+ +
Relative sharp boundary	+ + + + +	+ + + +
Seismic attributes		
Dip illumination	+ +	+ +
Edge content texture	+	+
Directionality	+ +	+ + +
Smoothness	+ + +	+ + + +
Chaos	+ + +	+ + +
Variance	+ +	+
Cosine of phase	+	+
Envelope	+ +	+
Energy	+ + + +	+ + + +
Instantaneous amplitude	+ + +	+ + +
RMS amplitude	+ +	+ + + +
Semblance	+ + +	+ + +
Grubbs filter	+ +	+ + +
Prewitt filter	+ + + + +	+ + + + +
GLCM variance	+ +	+ + + +
Gradient curvature	+ + +	+ + +

A wide literature study has performed to draw weights for each seismic attribute for exploratory and target functions (Bitrus et al. 2016; Nikoo et al. 2016; Soleimani et al. 2018a, 2018b; Anees et al. 2019; Boustani et al. 2019; Radfar et al. 2019; Anyiam and Uzuegbu 2020; Li et al. 2021)

+Means the weight (or quantity) of using selected parameter for buried channel detection

+++++Strongly related

++++Mostly related

+++Moderately related

++Weakly related

+Not related

attributes. The seismic attributes related to the identification of the channel system were divided into two groups, i.e., the seismic attributes that enhance the boundary of the channels, and the seismic attributes which identify the channel system based on the difference between the infilled channels sediments and the enclosing media. The first group of attributes are the Prewitt filter, the Grubbs filter, the GLCM variance and the curvature gradient. The second group of attributes consists of the similarity, the semblance, the energy, the instantaneous amplitude, and the RMS amplitude. As a first step of the workflow, these seismic attributes have been extracted from the seismic data in order to provide a primary insight on the channel system in the study field. Since Li et al. (2016) have stated that the CWT method provides better results for spectral decomposition, thus the CWT method has been applied on seismic data for spectral decomposition for frequencies between 20 and 45 Hz, with 5 Hz intervals. Investigation of these results will define in which frequency bands we can search for better identification of channel system. Meanwhile, a spectral decomposition step is required to be applied on the image and then extract the related attributes. This step is performed for all the frequency bands. herefore, for each attribute, there would be six attribute sections applied to single frequencies obtained by the CWT method. Investigation of the sections for each attribute will define the single frequency sections in which the selected attribute provides the best appearance of the channel system.

Afterward, the best three single frequency sections of each attribute that are applied on the CWT spectral decomposed data with the best appearance of the channel system, would be selected for composition by the RGB method. This combination provides six combined attributes cube that present different properties of the channel system and each cube enhances different parts of it. To have these advantages simultaneously on a combined cube, various combination of these CWT decomposed attribute for various single frequencies would be obtained by the RGB composition in order to have these advantages simultaneously on a combined cube. This strategy brings dozens of options for RGB composition of attributes. Figure 1 shows the proposed strategy to obtain the best possible composition of seismic-multi attribute by the RGB method, for buried channel detection.

Related attributes for buried channel detection

The continuous wavelet transform (CWT) was introduced to resolve deficiencies in providing high resolution of the short time frequency transform (STFT). In the CWT method, the seismic signal is multiplied by the wavelet function, which performs as the window function applied on the segments of the signal (Alaei et al. 2018). Since the Fourier transform is not applied in the CWT method, thus negative frequencies are not involved in the transformation. Additionally, the window's length varies by frequency in the CWT method. The CWT equation is as follows (Boashash 2015):

$$CWT_x^{\Psi} = \Psi_x^{\Psi}(\tau, s) = \frac{1}{\sqrt{|s|}} \int_{-\infty}^{+\infty} x(t)\Psi^*\left(\frac{t-\tau}{s}\right)dt \quad (1)$$

where τ and s are time shift and scale parameters that also define windows sliding length on the signal.

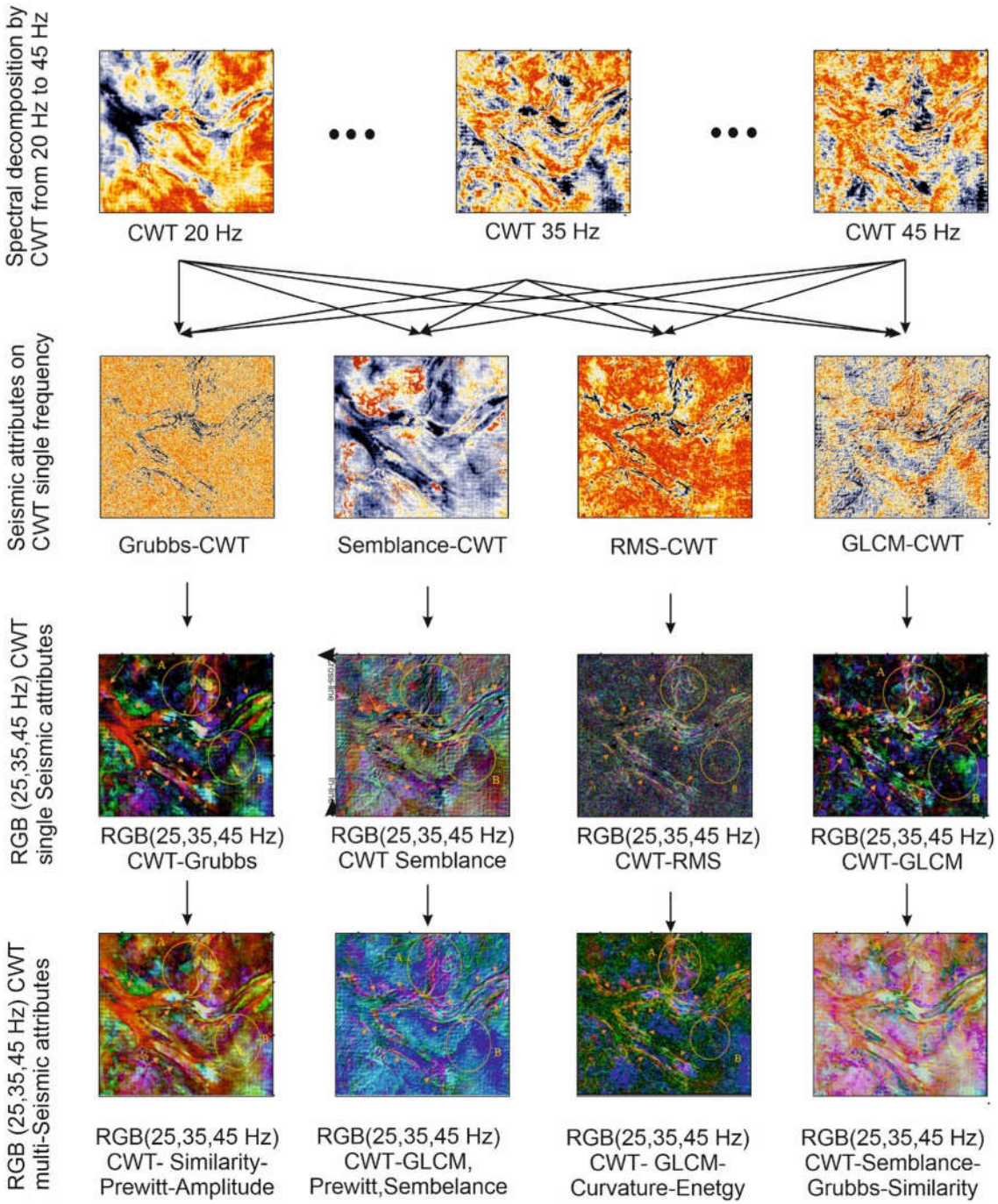

Fig. 1 Flowchart of the proposed strategy to obtain the best RGB combined seismic attribute for channel system identification on the seismic data

It should be noted that against the STFT method, the frequency parameter does not appeare in Eq. (1), but the scaling parameter is used, which has reverse relationship with the frequency. Large-scale values in the CWT method represent the general trend of the signal, without detailed information and the small-scale values reveal detailed variation of the seismic signal. The resolution of the CWT method in the time–frequency plane is limited by the Heisenberg's principle of uncertainty. The window function in the CWT method is used for the segmentation of the signal. The most important procedure here is to optimize the window's length, which is performed by the adaptive scale factor. Obviously, a small window's length is used for extracting information from high frequency components and large window's length

is used to reveal information from low frequency components. These frequency bands in the selected window's length could have coverage with each other. By definition, the mother wavelet is defined by the scale factor in the function, the window's length and the time lag of the window as (Boashash 2015):

$$\varphi_{\sigma,\tau}(t) = \frac{1}{\sqrt{\sigma}}\left(\frac{t-\tau}{\sigma}\right) \tag{2}$$

where σ is the scale factor and τ is the window's time length. Table 2 shows the steps of applying the CWT on the seismic signal. For large-scale factor, time resolution will increase. For small-scale factors, the signal will shrink in frequency direction and thus provide higher resolution in frequency domain. The following equation presents the CWT function as:

$$F(\sigma,\tau) = \frac{1}{\sqrt{\sigma}}\int_{-\infty}^{+\infty} f(t)\varphi^*\left(\frac{t-\tau}{\sigma}\right)dt \tag{3}$$

The final results are the optimized scale and transform factors that exhibit the highest similarity between the wavelet and the signal. There are various seismic attributes available to extract the required information from seismic data for precise delineation of the buried channels. Each of these attributes exhibit a special property of the buried channel, which have been described as it follows. The similarity attribute defines the similarity level of two adjacent seismic traces in the seismic data. The similarity value varies between 0–1. Obviously, a similarity value close to 1, presents a high level of similarity between two adjacent seismic traces and this value vanishes by reducing similarity between two traces, defined by (Barnes 2016):

$$\mathrm{S} = 1 - \frac{\sqrt{\sum_{i=1}^{n}\left(x_i - y_i\right)^2}}{\sqrt{\sum_{i=1}^{n} x_i^2 + \sum_{i=1}^{n} y_i^2}} \tag{4}$$

where x and y are two arbitrary seismic traces that their Euclidean distance vector is defined by $(x_i\text{-}y_i)^2$, divided by the sum of the vectors. The other wide applicable attribute for channel detection is the semblance attribute. It is defined by cross-correlation of two adjacent seismic traces to the selected central trace. The semblance value would be defined by Eq. (5) along with the spatial position (receiver line of seismic data of seismic traces, P_x, and in the time direction for traces in positions of x_i, y_i and x_{i+1}, y_i (Barnes 2016):

$$p_x(t,l,x_i,y_i) = \frac{\sum_{\tau=-l}^{+l} u(t-\tau,x_i,y_i)u(t-\tau-m,x_{i+1},y_i)}{\sqrt{\sum_{\tau=-l}^{+l} u^2(t-\tau,x_i,y_i)\sum_{\tau=-l}^{+l} u^2(t-\tau-m,x_{i+1},y_i)}} \tag{5}$$

where 2 l is the instantaneous time length of the correlation window. The cross-correlation value along the source line of the seismic data, P_y, and in the time direction for traces in positions of x_i, y_i and x_{i+1}, y_i would be (Barnes 2016):

$$p_y(t,m,x_i,y_i) = \frac{\sum_{\tau=-l}^{+l} u(t-\tau,x_i,y_i)u(t-\tau-m,x_{i+1},y_i)}{\sqrt{\sum_{\tau=-l}^{+l} u^2(t-\tau,x_i,y_i)\sum_{\tau=-l}^{+l} u^2(t-\tau-m,x_{i+1},y_i)}} \tag{6}$$

Like as the semblance attribute, the energy attribute could be used for detection of geological objects containing different sediments compared to the surrounding medium. This attribute, by definition, is the sum of the squared amplitudes within the time window (t_1, t_2) with an increment of τ in the window as:

$$\mathrm{E}(t,x,y,t_1+t_2) = \sum_{\tau=t_1}^{t_2} u(t+\tau,x,y)^2 \tag{7}$$

The energy attributes perform efficiently in the identification of gas chimneys and other geological objects, where amplitudes are distorted in a specific media due to the geological object. The instantaneous amplitude attribute which is widely used in seismic data interpretation, shows variation of the acoustic impedance, reveals and enhances the bright spot anomalies, mostly related to gas reservoirs and identifies the boundary of sequences. The instantaneous amplitude is defined by:

$$\mathrm{a}(t) = \sqrt{x(t)^2 + y(t)^2} \tag{8}$$

Table 2 Sequential steps that represent the CWT procedure

The procedure step		The performed analysis
Preliminary analysis	Step 1	Selection of a wavelet
	Step 2	Define a scale factor and shift the wavelet to the beginning of the signal
Main CWT analysis	Step 3	Compute the similarity between the shifted and scaled wavelet of the signal
	Step 4	Slide the wavelet with the preserved time and spatial resolution on the signal
	Step 5	Repeat the last to steps to reach the end of the signal length
Post CWT processing and signal extraction	Step 6	Reduce the scale factor and repeat the previous steps with new scale factor
	Step 7	Perform the calculation to extract the desired result

where $x(t)$ and $y(t)$ represent amplitude variations in x and y directions, respectively. The root mean square (RMS) amplitude is also another applicable attribute that by definition is the square root of the average of squared instantaneous amplitudes within a predefined range. The RMS amplitude attribute can clearly identify bright spots, amplitude anomalies and the seismic velocity variations independent from the local reflector dips. This attribute also defines variations in seismic facies related to coarse sediments, compared to fine sediments, such as shale and fine sands. The RMS amplitude is defined by (Barnes 2016):

$$X_{RMS} = \sqrt{\frac{1}{N}\sum_{n=1}^{N} w_v x_n^2} \tag{9}$$

where N is the sample number, w is the window length and x is the instantaneous amplitude value. The other effective attribute known as the Prewitt seismic amplitude is mostly known as a filter to enhance contrasts between geological objects and the surrounding media. The Prewitt amplitude calculates dip of seismic events in different directions in an analyzing cube with $3\times3\times3$ pixel size. The other applicable attribute is the Grubbs filter, which is a statistical approach for defining anomaly or outliers in a normalized variable. This attribute could define outstanding anomalies of any specific property of the geological object. This attribute could efficiently enhance seismic objects with sufficient contrast in a specific seismic property with the enclosed media. Similarly, the variance of the grey level matrix in texture definition of a seismic attribute, defines the variation of the texture properties within a predefined pixel and its surrounding pixels. For a better definition of variation, mostly the covariance matrix is computed, therefore it could be called the grey level covariance matrix (GLCM) and by definition, it is calculated by the following equation (Chopra and Marfurt 2007):

$$\sigma_i^2 = \sum_{i,j=0}^{N-1} P_{i,j}(i-\mu)^2 = \sum_{i,j=0}^{N-1} P_{i,j}(j-\mu)^2 \tag{10}$$

where $P_{i,j}$ is the selected pixel and N is the number of samples. The GLCM value is symmetrical for different directions and thus same value would be obtained for $P_{j,i}$. Obviously, the curvature of geological objects should be defined in all direction precisely to build a comprehensive geological model of the subsurface media. Therefore, the gradient curvature attribute is proposed to define variation in curvature in all directions. The gradient curvature could be used for definition boundaries of the buried channels, if the channel filled sediments and the enclosed media has significant contrast in seismic properties. The gradient curvature attribute in 3D seismic cube is defined by (Barnes 2016):

$$k'_{2D} = \frac{d}{dx}\left[\frac{\frac{d^2z}{dx^2}}{(1+\left(\frac{dz}{dx}\right)^2)^{3/2}}\right]\frac{dx}{ds} = \frac{\frac{d^3z}{dx^3}}{\left(1+\left(\frac{dz}{dx}\right)^2\right)^{5/2}} - \frac{3\left(\frac{d^2z}{dx^2}\right)^2\frac{dz}{dx}}{\left(1+\left(\frac{dz}{dx}\right)^2\right)^{7/2}} \tag{11}$$

where k'_{2D} shows the gradient of curvature in desired directions, x and z. In the subsequent section, the aforementioned attributes would be applied on a synthetic and field 3D seismic data cube within the proposed strategy, to obtain the best possible image of the buried channel system.

Application on synthetic seismic data

To evaluate the proposed strategy, it is initially applied on a synthetic data. The synthetic seismic data was obtained over a geological model containing a channel, using dynamic ray tracing to generate the synthetic seismograms, adding random Gaussian noise to resemble real seismic data and applying the conventional seismic data processing to obtain the final seismic image for further application. Figure 2a shows the earth model and Fig. 2b illustrate the final simulated seismic image.

To initiate the proposed strategy, the CWT method was applied on the data in a frequency range from 5 to 90 Hz, with 5 Hz interval. Then initial analysis in these CWT images was performed to define the best frequency band, exhibits the best possible image of the channel. However, due to the large number of figures, only the selected images are presented here. It should be mentioned that the frequencies were selected based on deep and wide study on frequency sections with initially large and then small increment, providing large number of sections to investigate. Although it was not performed for all the attributes, but initially for most of the relevant one, and then the increment between the frequencies were decreased step by step to select the best frequency bands. Then in the spectral images it was observed that some parts of the channel are illustrated better at low, some at mid and others at higher frequencies. However, between 20 and 45 Hz frequency, clearer images of different parts of the channel were observed. These frequencies, at which the channel geometry is clearly pronounced, then were used for more investigation. Since different parts of the channel features are resolved at different frequencies, it was considered that the channel geometry can be obtained in its complete form when the different frequencies are stacked. Manual interpretation the proved that a stacked frequency volume obtained by summing up the 25 Hz (low frequency), 35 Hz (mid frequency) and 45 Hz (high frequency) volumes provides the best results, shown in Fig. 3a–c. The CWT image for 45 Hz does not provide a reliable image. However, it was the best image for the high frequency band obtained for this data. This procedure was applied also on the field

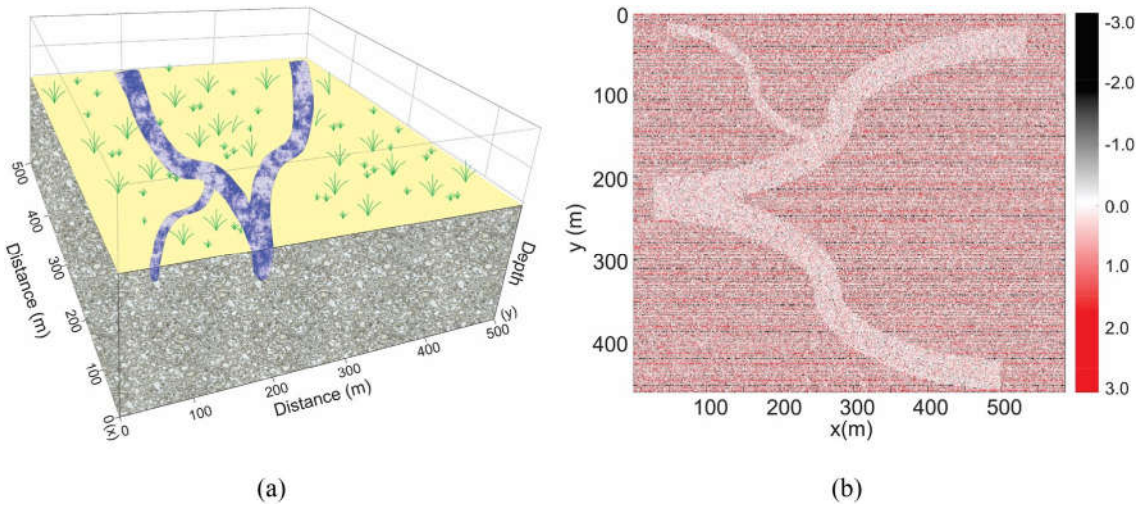

Fig. 2 **a** The earth model of a channel system used to generate the synthetic seismic data. **b** The simulated seismic image obtained from the synthetic seismic data

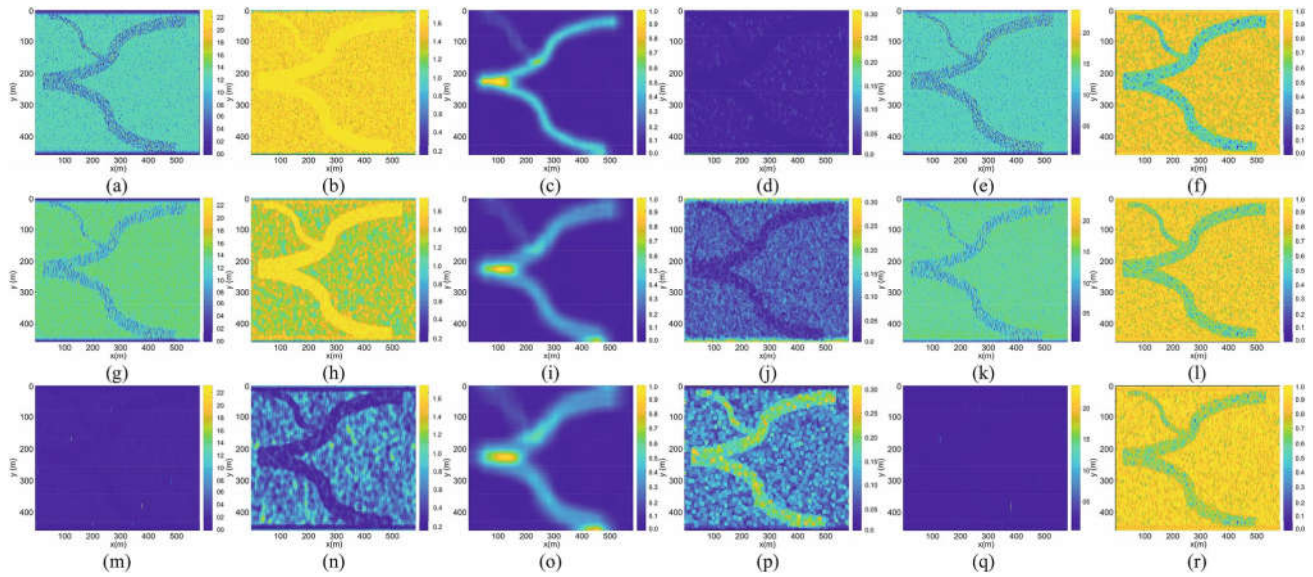

Fig. 3 The top raw show all the attributes for 25 Hz, the middle raw for 35 Hz and the bottom raw for 45 Hz. All the attributes are extracted from the CWT images, rather than the original image. Attributes from (**a**–**f**) are the CWT itself, the GLCM, the RMS, the semblance, the amplitude and the entropy. The same sequence of attributes is used for figures (**g**–**l**) for the 35 Hz and also for (**m**–**r**) for 45 Hz

data example. Then the GLCM, RMS, the semblance, the amplitude and the entropy attributes were applied on the CWT images. Figure 3 show the extracted attributes from the synthetic image. In Fig. 3, the top raw shows the CWT and all other attributes that extracted on the CWT image for 25 Hz frequency. The middle raw in Fig. 3 shows the same attributes but for the 35 Hz and the bottom raw for the 45 Hz. It is obvious that not all the extracted attribute could accurately image the body and the boundary of the buried channel. In the low frequency attributes, the GLCM and the semblance attributes (Fig. 3b, d) could not depict the buried channel, while other attributes for the 25 Hz frequency could better exhibit the channel. For the middle band frequency, the RMS and the semblance attributes (Fig. 3i, j) failed to properly illustrate the buried channel, while other attributes obtained on the CWT image could better image the target under investigation. In high frequency range, the CWT itself, the RMS and the amplitude attributes (Fig. 3m, o, q) could not image the buried channel. The seismic attributes of the GLCM and entropy, (Fig. 3n, r) could somehow illustrate

the channel, however, best result for the frequency range was obtained by the semblance attribute (Fig. 3p). It should be noted that much more attributes were extracted from the CWT images; however, they are not all shown here due to the large number of figures, but some of them might be later used in the RGB. Individual selection of the attributes might not be appropriate for target identification. Therefor they were combined through the RGB illustration method, for better identification of the target. Initially, the RGB images are obtained by simple combination of each selected attribute. Therefore, in each individual attribute, the 25 Hz image is selected as the red, the 35 Hz as the green and the 45 Hz as the blue components.

Figure 4 shows the RGB representation of the single attributes on the CWT image. Among the RGB images, the related RGB for the energy could not image the channel (Fig. 4d) and the RGB images for the GLCM, RMS and the semblance (Fig. 4f–h, respectively) could not illustrate the small branch of the channel. The RGB images for smoothness, edge and entropy (Fig. 4a, c, e, respectively), could illustrate the channel to some extent, but the amplitude RGB representation (Fig. 4b) could better image all parts of the channel with sufficient contrast.

In the next step, according to the RGB representation of the attributes and also performance of their individual frequency, large number of RGB representations are obtained by various combination of single frequency of various attributes. To have a comprehensive image of details of the channel, all the information laid in all frequency bands have to be integrated. Therefor for all the RGB representation, the red component is the 25 Hz single frequency of the selected attribute, the green component is the 35 Hz image of the attribute and the blue component is the 45 Hz image of the used attribute. Results of this combination are presented in Fig. 5. The combination of the GLCM, the smoothness and the edge, as the red, green and blue component, with the 25, 35 and 45 Hz frequencies, failed to represent the channel system (Fig. 5b). The combination of the RMS, the semblance and the similarity (Fig. 5c) and the combination of the semblance, the RMS and the GLCM (Fig. 5f), could not illustrate the small branch of the channel system. The combination of the smoothness, the edge and the similarity (Fig. 5e) could somehow image the channel system, but suffers from accurate definition of its boundary. By comparison of results, it can be concluded that the combination of the entropy, the edge and the smoothness (Fig. 5a) and the similarity, the GLCM and the smoothness (Fig. 5d) could better identify the channel system.

Application on 3D seismic data

The selected field seismic data for application of the proposed strategy is a 3D seismic cube acquired on a petroleum field in the south-western sector of Iran, known as the Dezful embayment. The selected petroleum field contains gentle dipping anticlinal structural trap. It can be assumed that there might be stratigraphic traps exists in the field (Soleimani 2013). The seismic data were interpreted, aiming at the identification of geological structures for stratigraphic tarps. Figure 6a shows location of the study field and Fig. 6b depicts the stratigraphical column of the region. Figure 6c shows a block diagram of the Middle Cretaceous that shows the complicated channel system, which is known as a possible stratigraphical oil trap. In the western part of the Dezful

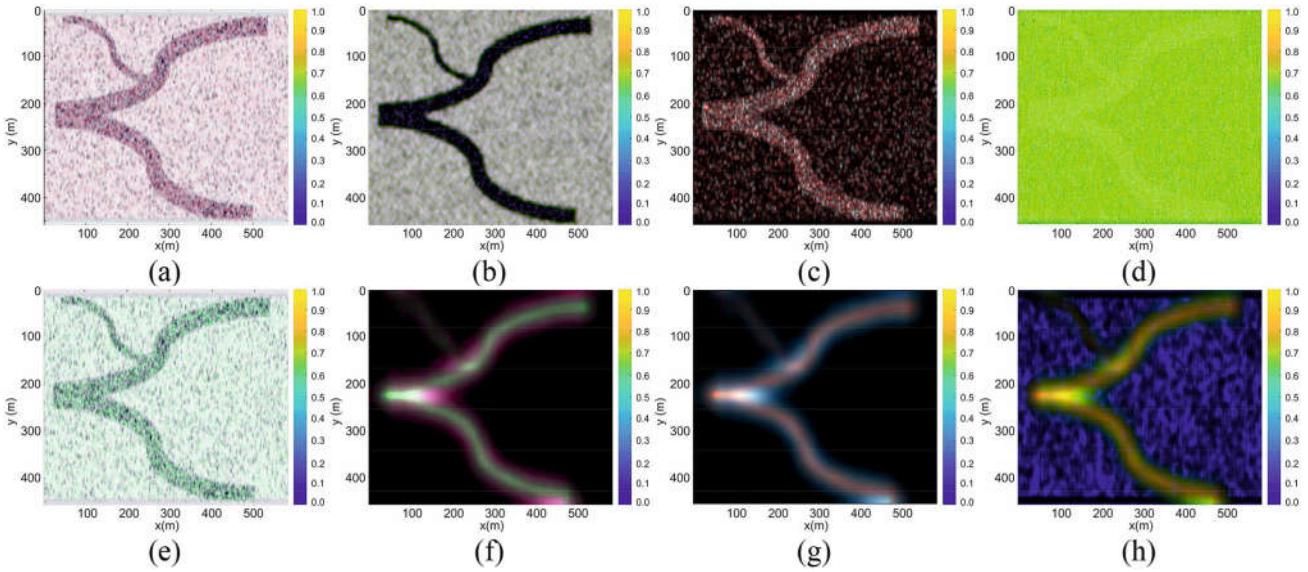

Fig. 4 The RGB representation of the individual attributes extracted from the CWT image

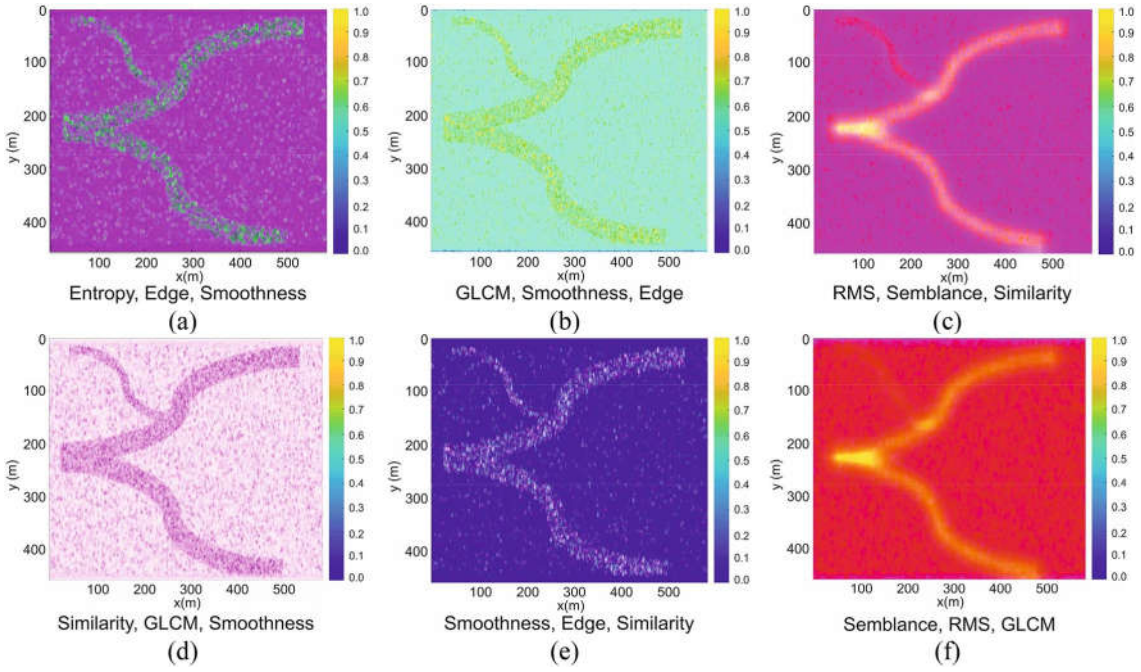

Fig. 5 **a–f** RGB representation of the various attributes. Each image contains respectively the 25, 35 and 45 Hz of the selected attribute as the red, green blue component

Embayment, there is no outcrops of rocks and the geological information are entirely derived from subsurface investigations. The structural and stratigraphic features of the Dezful Embayment have been well documented as a simply folded belt and foothills zone of the Zagros Basin (Atashbari et al. 2018). During the Early Cretaceous shallow marine carbonate sediments of Fahliyan Formation were deposited in the greater part of the Dezful Embayment. The depositional environment of the Early Cretaceous was mainly a shallow marine carbonate platform dipping gently eastward, forming a ramp over the Jurassic evaporites, however interrupted by episodes of clastic sedimentation consisting of massive and thin bedded limestone (AlShuaibi and Khalaf 2011).

The oldest Cretaceous units consists of interbedded sandy limestone, dark gray shale and silty shale, variegated limestone and black calcareous shale. The unit represents deep marine depositional environments (Wang et al. 2019). The Fahliyan Formation contains corals and algae, indicate deposition in a shallow, carbonate shelf environment. The Gadvan Formation consists of dark-gray, argillaceous bioclastic limestone interbedded with gray, green to brownish-yellow marl. Lateral facies changes occur in the formation of dark shale and argillaceous limestone, to the dark argillaceous limestone and ranges in deposition from a shallow marine to neritic, inner-shelf, lower energy environment (Shahbazi et al. 2020). The Kazhdumi Formation formed an unconformity at the Aptian-Albian boundary with fine clastic terrigenous sediments deposited. This formation forms a major progradational deltaic complex. The Kazhdumi Formation has sandstone layers in its basal part and is considered as the source rock for oil in the Dezful Embayment (Atashbari et al. 2018). The Sarvak Formation was deposited in a shallow marine environment and consists of shallow marine sediments that change into low energy shaly sediments towards the south. The upper boundary of the Sarvak Formation differs from place to place. The Sarvak and the overlying Ilam formations form an extensive limestone unit that is interpreted to have been deposited in shallow and neritic environments and an erosional unconformity between these two formations are observed (AlShuaibi and Khalaf 2011). Since the application of the proposed strategy with a large number of seismic attributes, selected to be extracted, requires large computation time to be applied on whole seismic data, only the part of the seismic cube including the buried channel was selected to be used in this study. The seismic data cube that was cropped from the whole seismic data contains 608 xlines and 674 inlines, depicted in Fig. 7a. The 1800 ms time slice, where the best image of the buried channel is observed, is shown in Fig. 7b. The selected seismic attributes are the energy, the instantaneous amplitude, the RMS amplitude, the Prewitt filter, the Grubbs filter, the similarity, the semblance, the GLCM variance and the gradient curvature.

Results of applying these attributes to the seismic data are depicted in Fig. 8. As it could be seen, the seismic attributes which enhances the channel's boundary perform better in

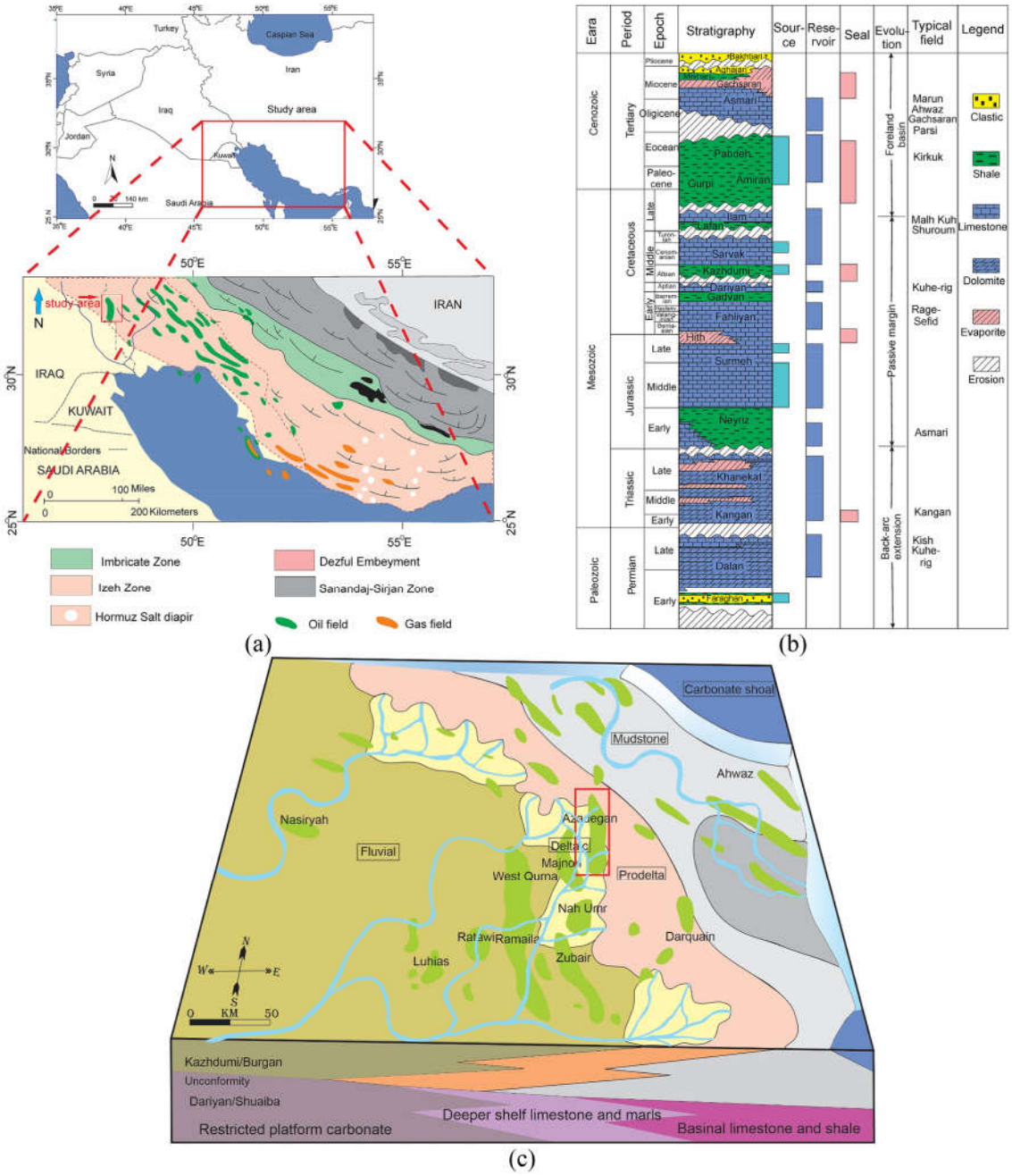

Fig. 6 **a** Location of the selected petroleum field and the 3D seismic data. **b** The stratigraphic column of the study field. **c** The block diagram of the study area for the middle Cretaceous, when the channel system was active

the identification of the channel system, if compared with the attributes that separate the channel system based on the textural attributes of the sediments infilling the channel. It is due to the reason that there are fewer differences between the sand-filled channel sediments and the surrounding media, which consists of shaly sands.

However, the channel system is not well identified by a single attribute analysis, but it could be improved to identify all details of the buried channel. Subsequently, the spectral decomposition procedure was applied on data to extract the single frequency sections by the CWT method. This procedure was applied by a Morlet wavelet with frequencies from 10 to 90 Hz, with 5 Hz increment. After investigation of result on applying the spectral decomposition, it was observed that appropriate results were obtained for spectral decomposition by the CWT method for frequencies of 20, 25, 30, 35, 40 and 45 Hz. Figure 9 shows the results of this investigation on appropriate extraction of single frequency

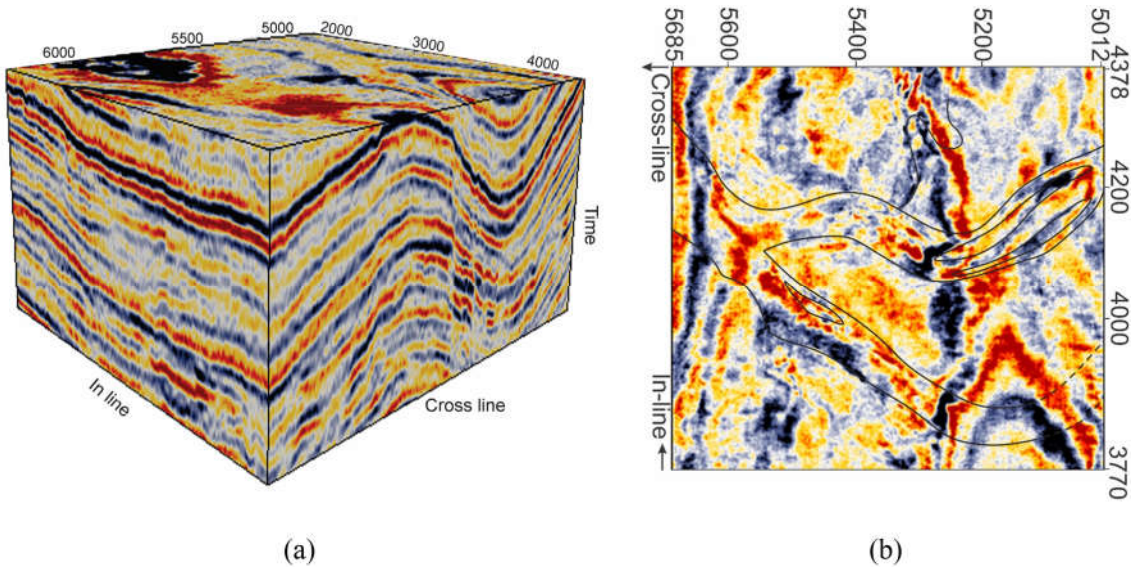

Fig. 7 **a** The 3D cube of the selected seismic data in this study and **b** the 1800 ms time slice, where the buried channel exhibits the most outstanding appearance. The interpreted channel from the final result is overlayed on the seismic time slice here

sections by the CWT spectral decomposition method. As it could be seen, the results of the CWT spectral decomposition for frequencies of 20 and 25 Hz reveal the main branches of the buried channel, while results for the 30 and 35 Hz frequencies reveal the minor branches of the channel system. However, for the time slices obtained for 40 and 45 Hz, only some parts of the main branch of the buried channel have been identified. Subsequently to enhance result of the identification the single channel on single frequency time slices obtained by the CWT spectral decomposition method, the common seismic attributes were had been applied. To select the best results, more than 20 seismic attributes have been applied on time slices with single frequencies of 20–50 Hz, with a 5 Hz increment. Among these attributes, only the results of applying the energy, the instantaneous amplitude, the RMS amplitude, the Prewitt filter, the Grubs filter, the similarity, the semblance, the GLCM variance and the gradient curvature have been selected for illustration. Also based on the result of spectral decomposition, only results of applying attributes on time slices of 25, 35 and 45 Hz single frequencies are illustrated here. Figure 10 illustrate the 25 Hz single frequency time slice for all the aforementioned attribute. The CWT-energy attribute could identify the major channels, and could not detect the small branches in the channel system (Fig. 10a). The CWT-instantaneous amplitude and the CWT-RMS amplitude (Fig. 10b, c), illustrate the almost same image. They could define the major channels, with a better definition of the variation in channel infilled sediments, possibly due to the size of the infilling sediments, changing their amplitudes. To better detect the channels boundary on the CWT single frequency image, the Prewitt filter was applied. Figure 10d shows the result of applying the Prewitt filter on 25 Hz single frequency image obtained by the CWT method. As it could be seen, the channel's boundary could be identified well in the northern part of the area. However, in the southern part, there is a low contrast between the infilled and the surrounding sediments, and less contrast was observed for the inner and outer channel media. Therefore, the boundary could not be identified well, while there is some added operator noise to the section.

The Grubbs filter was also applied to enhance the minor branch and clearly identify the borders of the main channel. The graphs resulting from the application of the Grubbs filter on the 25 Hz single frequency decomposed time slice are presented in Fig. 10e. The time slice does not exhibit operator added noise, and the main branch have been clearly identified. The southern branch of the channel system was also well defined, while some evidences of the minor branches have also been detected, which fed both the northern and southern branches. The similarity attribute applied on the CWT decomposed image for 25 Hz single frequency image is depicted in Fig. 10f. The similarity attribute defines the inner channel media based on the difference of sedimentation with the outer channel. This attribute could efficiently detect the southern branch of the channel system, too. The semblance attribute uses almost the same definition of the similarity, and corresponding results (25 Hz single frequencies) have identified the main branches of the channel system (Fig. 10g). The GLCM-variance and the curvature gradient are both known as edge enhancement attributes. Therefore, it was assumed that by applying these attributes on the 25 Hz

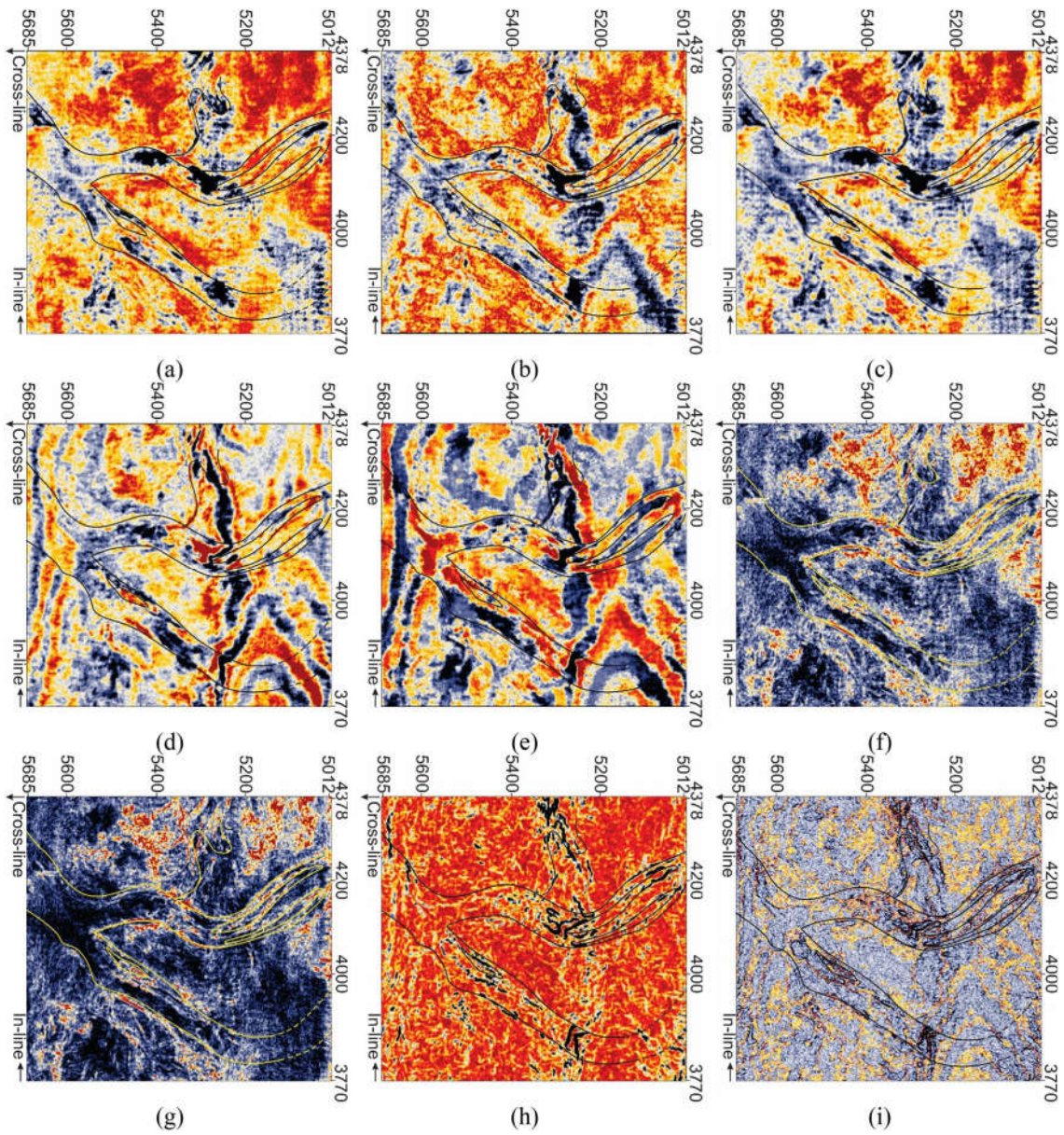

Fig. 8 Extraction of the common seismic attributes related to enhancement of buried channel. **a** the energy, **b** the instantaneous amplitude, **c** the RMS amplitude, **d** the Prewitt filter, **e** the Grubbs filter, **f** the similarity, **g** the semblance, **h** the GLCM variance, and the **i** curvature gradient attributes. The interpreted channel from the final result is overlayed on the seismic time slices here

single frequency decomposed by the CWT method, the boundaries of the channel system would be easily identified.

Results of applying the GLCM variance and the curvature gradient are represented in Fig. 10h and i, respectively. As it could be seen, the channel's boundary has been well identified, and some evidences of the minor channels in the northern part of the area have been observed. Figure 11 shows the same procedure of applying the aforementioned attributes on the 35 Hz single frequency decomposed data. The 35 Hz CWT-energy attribute could identify the variation in the infilling sediment through the main branches of the channel (Fig. 11a). However, the main channel system could not be clearly predicted as for the 25 Hz single frequency section. The 35 Hz CWT-instantaneous amplitude and the 35 Hz CWT-RMS amplitude (Fig. 11b, c), could not clearly identify the main branches. However, they have better defined the minor branches of the channel system and also exhibit detail variations inside the channel system. The 35 Hz CWT-Prewitt and the CWT-Grubbs filter have also identified detailed variations in the channels border (Fig. 11d, e).

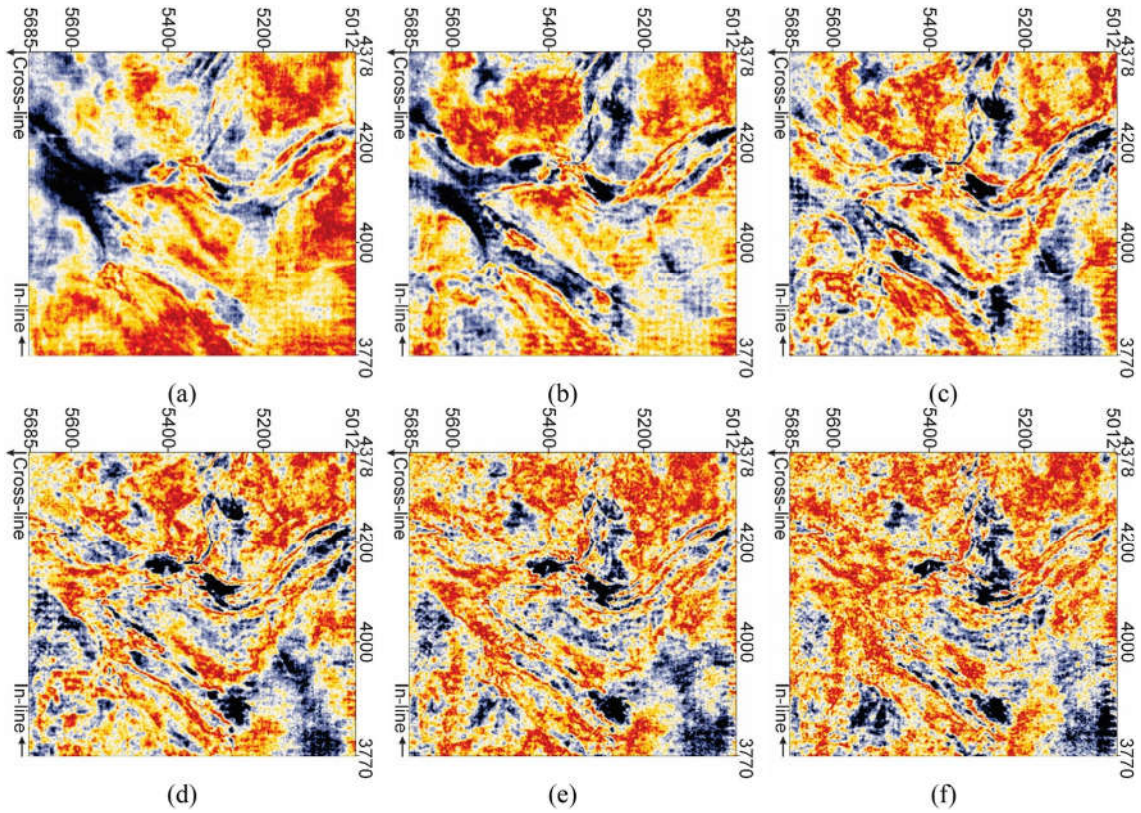

Fig. 9 The CWT spectral decomposition of data with single frequencies of **a** 20 Hz, **b** 25 Hz, **c** 30 Hz, **d** 35 Hz, **e** 40 Hz, and **f** 45 Hz

The CWT-Prewitt filter less suffers from the added operator noise, so representing the first image that could clearly identify the minor branch of the channel system in the northern sector. The CWT-similarity and CWT-semblance attributes for 35 Hz single frequency are represented in Fig. 11f and g. The CWT-similarity section exhibits different seismic textures in the image, that can be used for further interpretation. The boundaries of the main branches are also well defined and some evidences of minor branches are also illustrated. The CWT-GLCM variance and CWT-curvature gradient for 35 Hz single frequency are depicted in Fig. 11h and i. These two sections clearly identified the minor branches, specifically in the north of the section, although the channel's borders of the major branches could not be detected well. The channel system is not well defined in the CWT-energy attribute for 45 Hz single frequency image, however, variation of seismic pattern due to changes in the infilled channel sediments are clearly identified. The CWT-instantaneous amplitude and the CWT-RMS amplitude for 45 Hz single frequency images were also obtained for the study seismic data. However, neither the borders of the channel's system, nor the major and minor branches are well defined by these attributes. Therefore, these two results are not shown here and are not used for further combination. For better identification of the buried channels, the seismic images obtained by applying common attributes on the results of the CWT spectral decomposed data were combined by the RGB technique. This combination was performed by two strategies. The first strategy consists of combination results of a single attribute but with different frequencies. The second strategy is to analyze results of the first strategy and combine various attributes with different frequencies. These two strategies would be explained and applied on data in the subsequent images.

RGB composition of single seismic attributes

In this strategy, the CWT spectral decomposition results for frequencies of 25, 35 and 45 Hz for each attribute have been selected for the RGB combination. In all the combinations, the single frequency sections of 25 Hz was selected as the red component, the single frequency section of 35 Hz as the green and the section of 45 Hz single frequency section as the blue components. The first selected attribute for the RGB combination was the similarity attribute. By the RGB combination of the similarity attribute, the minor branches of the buried channel were clearly enhanced and identified, shown by yellow circles in Fig. 12a. The main branch of the buried channel was also well identified. The semblance attribute has been selected as the other attribute for

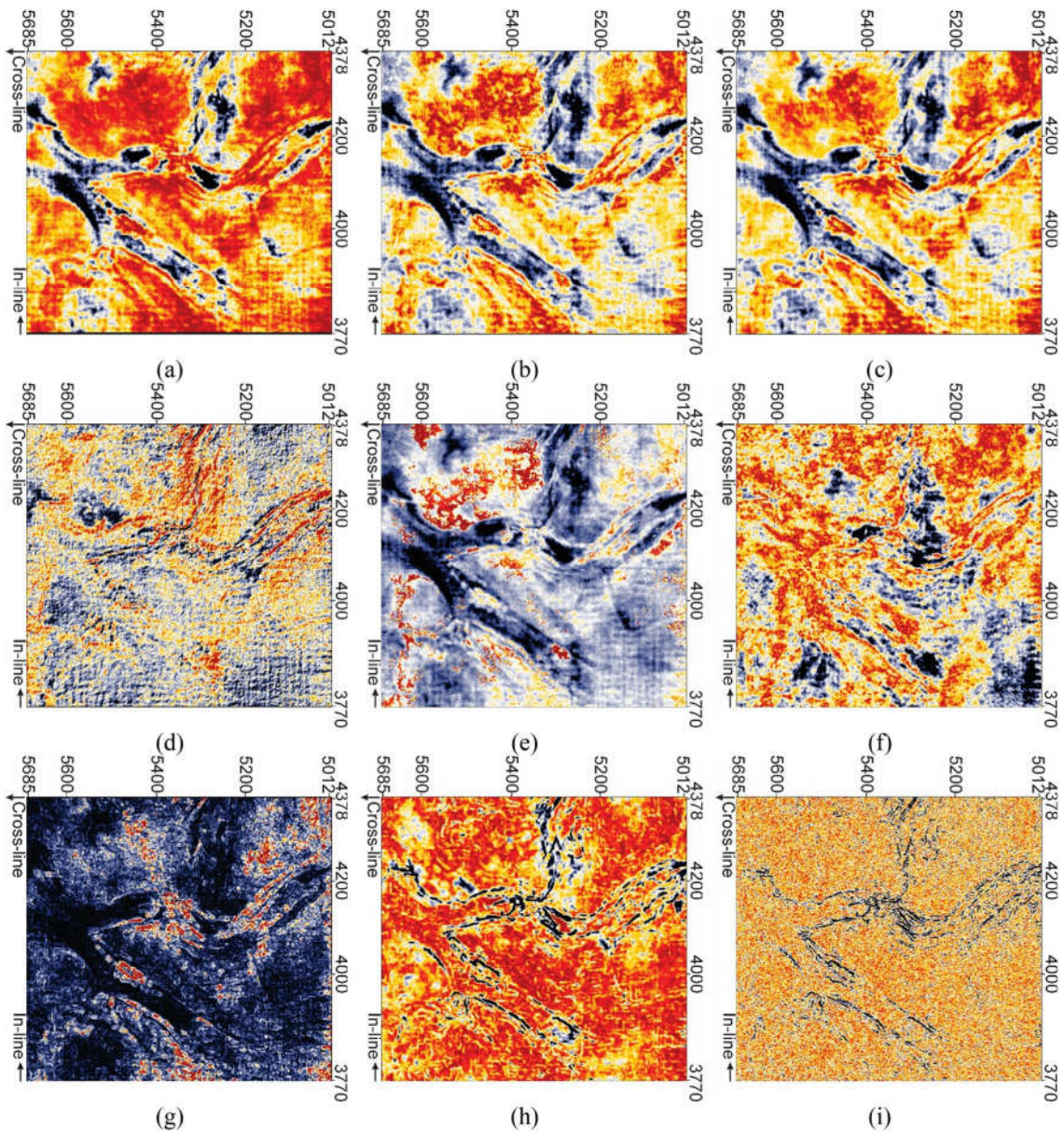

Fig. 10 Result of applying the proposed attributes on the 25 Hz single frequency seismic time slice obtained by the CWT method. These attributes are **a** the energy, **b** the instantaneous amplitude, **c** the RMS, **d** the Prewitt filter, **e** the Grubbs filter, **f** the similarity, **g** the semblance, **h** the GLCM variance, and **i** the gradient curvature

the RGB combination. The RGB combined section for the CWT-semblance attribute (Fig. 12b) could efficiently separate internal part of the buried channel from the enclosing medium, and thus could better identify the main branches of the channel system. The results show that the boundaries of the buried channel were identified more better by the RGB composition of the CWT-semblance attribute, although it cannot clearly identify the minor branches. Result of applying the RGB combination on the components of the CWT-RMS amplitude is depicted Fig. 12c. Minor branches of the buried channel is obvious in this RGB compound image and the channel boundary and its internal variation are also well identified. It was the case also for the RGB combination of the CWT-energy attributes, where minor branches of the channel system are clearly identified, depicted in Fig. 12d. The boundary of the main branch was also clearly depicted by this image. The RGB combination of the CWT-Grubbs filter is illustrated in Fig. 12e. Its result, however, is not promising compared to the previous results obtained by other attributes. The CWT-instantaneous amplitude RGB combination result is depicted in Fig. 12f. The combined RGB section of the CWT-instantaneous amplitude could

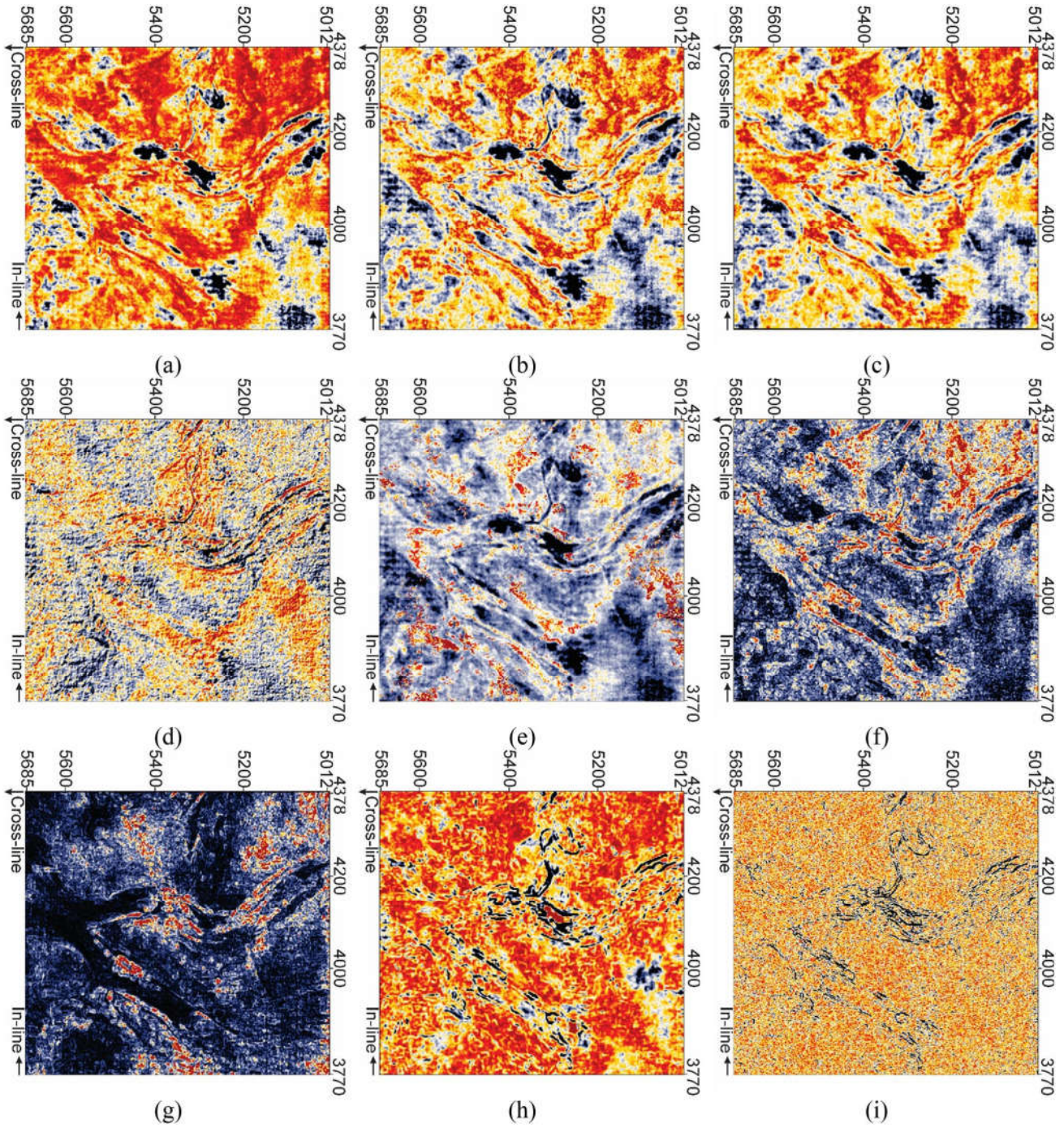

Fig. 11 Result of applying the proposed attributes on the 35 Hz single frequency seismic time slice obtained by the CWT method. These attributes are **a** the energy, **b** the instantaneous amplitude, **c** the RMS, **d** the Prewitt filter, **e** the Grubbs filter, **f** the similarity, **g** the semblance, **h** the GLCM variance, and **i** the gradient curvature

clearly reveal the geometry of the small branches of the buried channel and also the internal variation of the main channel, which is obvious by variation of its color. However, accurate boundary of the main channel is not well defined by the RGB combination of this attribute. As the CWT-Prewitt filter attribute is a filter to enhance edges of the geological objects, therefore, it is assumed that the RGB combination of its components clearly image the boundaries of the channel. Results were promising by investigating the RGB combination of the CWT-Prewitt filter (Fig. 12g). Boundaries of the upper minor and major branches of the buried channel system are well defined by this attribute. However,

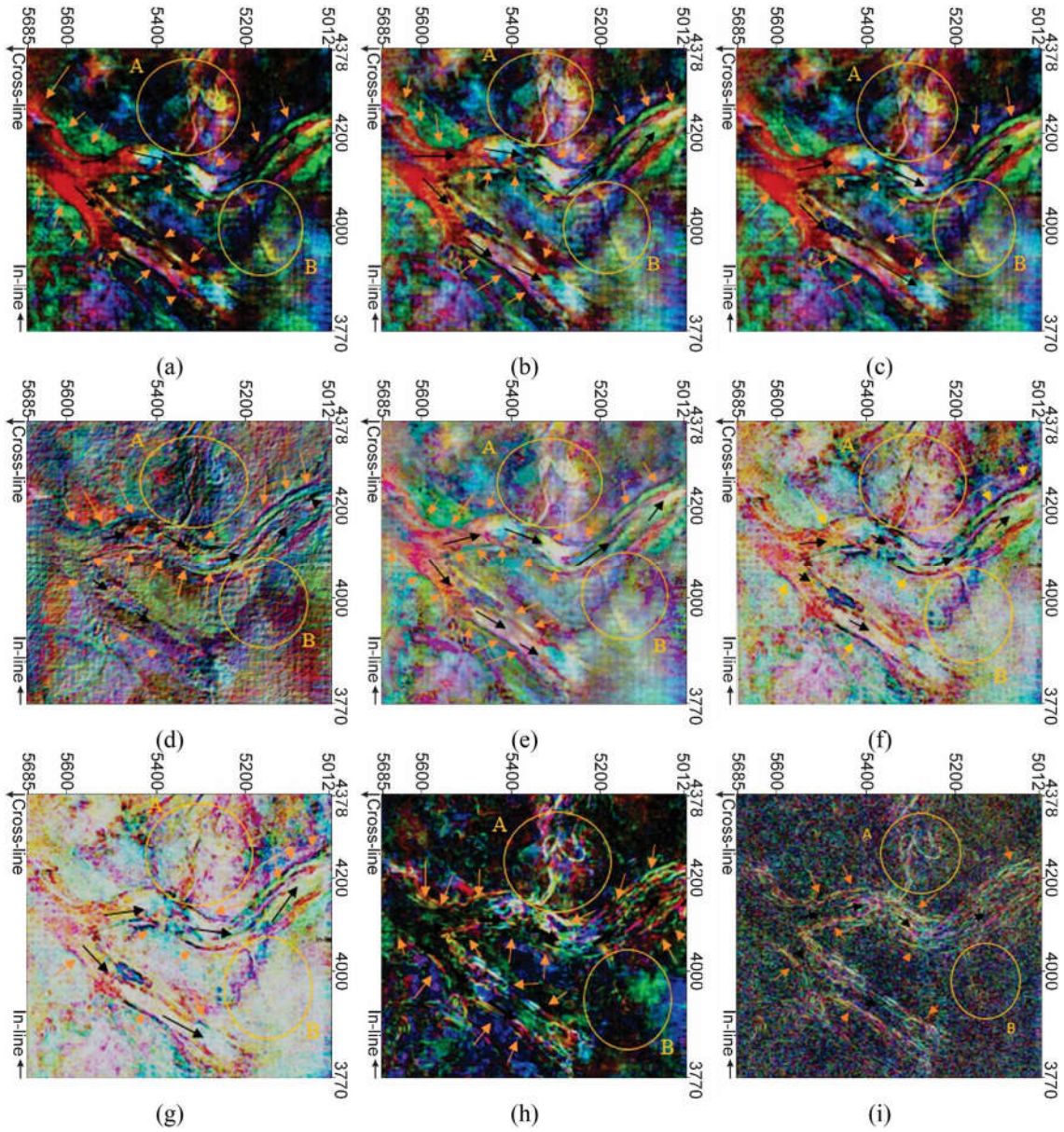

Fig. 12 Result of the RGB combination on attributes extracted from the CWT decomposed images. For all the attributes, 25, 35 and 45 Hz single frequency sections were selected as red, green and blue components, respectively. **a** The CWT-energy, **b** the CWT-instantaneous amplitude, **c** the CWT-RMS, **d** the CWT-Prewitt filter, **e** the CWT-Grubbs filter, **f** the CWT-similarity, **g** the CWT-semblance, **h** the CWT-GLCM variance, and **i** the CWT-gradient curvature attributes

due to the low contrast between the infilling channel sediments and the enclosing media in the lower branch of the channel, this attribute could not precisely perform the edge enhancement procedure. The GLCM variance attribute is a textural attribute, supposed to reveal and enhance seismic textural properties of the internal channel. By investigation on the RGB combined image of the CWT-GLCM variance attribute, it was observed that the internal properties of the buried channel were clearly imaged (Fig. 12h). However, the channel boundary is not sharp in Fig. 12h, since the GLCM variance attribute is not an edge enhancement attribute. The RGB combination of the CWT-gradient curvature have been identified the boundary of the buried channel (Fig. 12i). As it could be seen, boundaries of both minor and major branches of the channel's system are clearly identified. However, this attribute could not differentiate the internal and external channel media.

RGB composition of multi-seismic attribute

In this strategy, the red, the green and the blue components in the RGB combination procedure have been selected from various attributes. Selection of each component from different attributes is based on using advantage of each attribute in enhancing a specific property of the channel system. In the first combination procedure, the 25 Hz single frequency section of the CWT-similarity was selected as a red component, the 35 Hz single frequency section of the CWT-Prewitt as a green component and the 45 Hz single frequency section of the instantaneous amplitude attribute was considered as a blue component (Fig. 13a, b). The major channel and its boundary have been clearly imaged in the most parts, except the southern sector of the channel boundary, due to the low contrast between the inner channel media and the outer sediments. To build the RGB image, the 25 Hz CWT-Prewitt filter, the 35 Hz CWT-similarity and the 45 Hz CWT-Grubbs filter are selected as the red, the blue and the green components, respectively.

Its 2D combination is depicted in Fig. 13c and the 3D combination in Fig. 13d. The boundary of the channel for both the major and the minor branches are well imaged and efficiently enhanced. To identify the channel boundary and the inner sand-filled channel system from the enclosed media, advantage of the Grubbs filter and the similarity attribute were used in the RGB combined attribute image (Fig. 14a, b). Here the CWT-semblance for 25 Hz, the

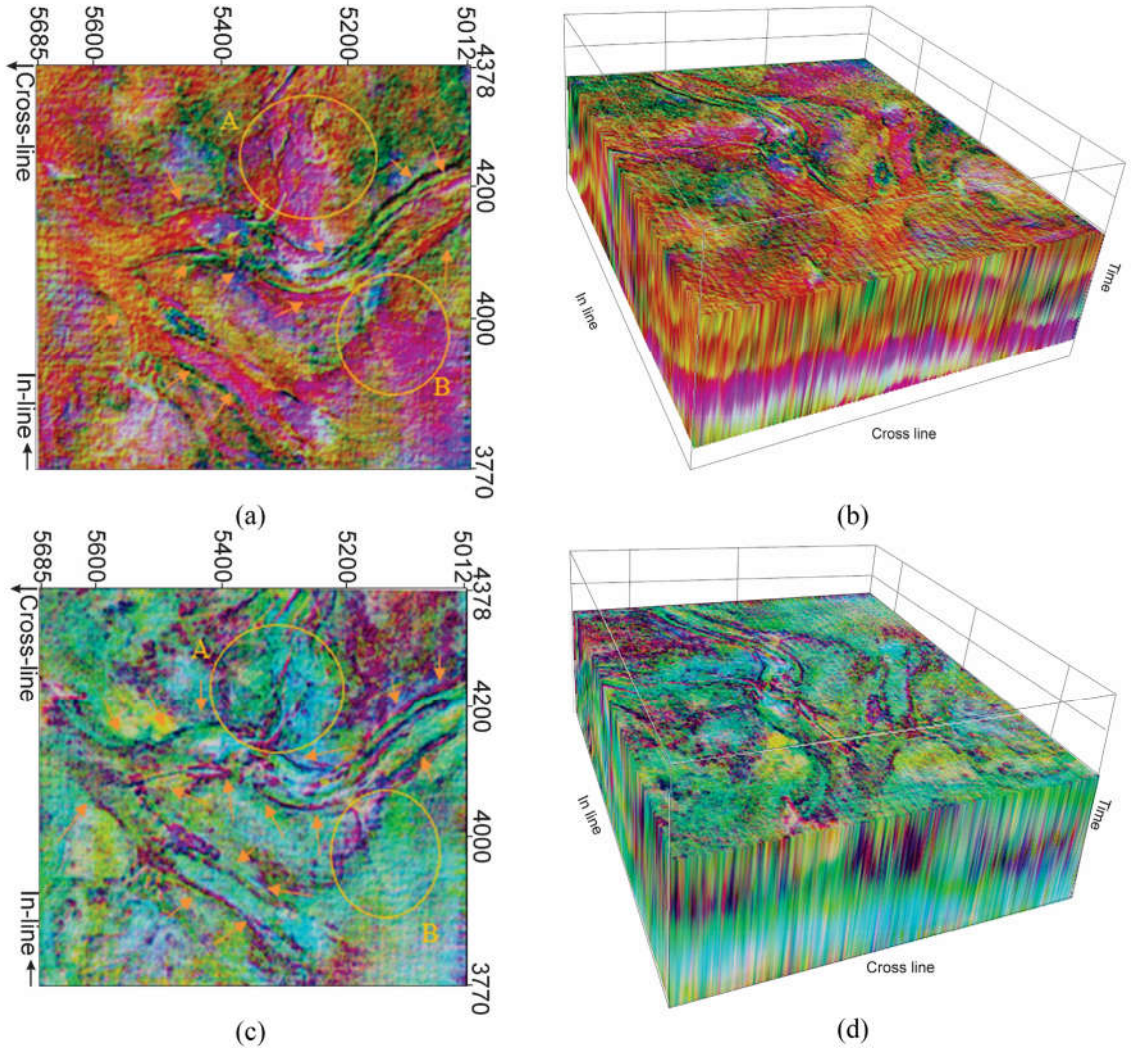

Fig. 13 **a** Representation of the time slice with the RGB composition of the CWT-similarity for 25 Hz as the red, the CWT-Prewitt for 35 Hz as the green and the CWT-instantaneous amplitude for 45 Hz as the blue component. **b** The 3D RGB composition with the same components as in (**a**). **c** Representation of the time slice with the RGB composition of the CWT-Prewitt for 25 Hz as the red, the CWT-similarity for 35 Hz as the green and the CWT-Grubbs filter for 45 Hz as the blue. **b** The 3D RGB composition with the same components as in (**c**)

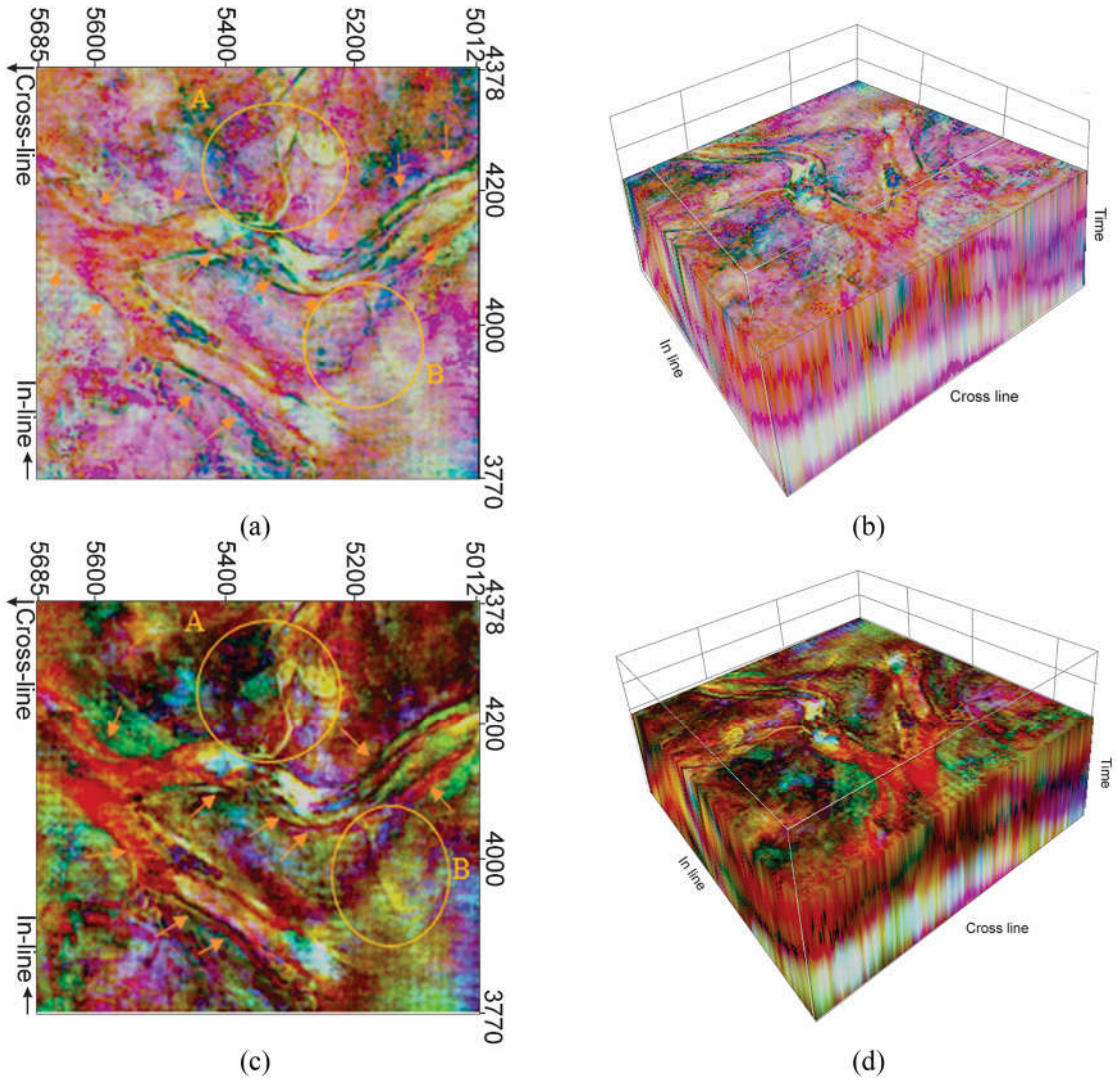

Fig. 14 **a** Representation of the time slice with the RGB composition of the CWT-semblance for 25 Hz as the red, CWT-Grubbs for 35 Hz as the green and CWT-similarity for 45 Hz as the blue components. **b** The 3D RGB composition with the same components as in (**a**). **c** Representation of the time slice with the RGB composition of the CWT-Grubbs for 25 Hz as the red, CWT instantaneous amplitude for 35 Hz as the green and CWT-energy filter for 45 Hz as the blue component. **d** The 3D RGB composition with the same components as in (**c**)

CWT-Grubbs filter for 35 Hz and the CWT-similarity for 45 Hz were selected as the red, the green and the blue components, respectively. The result obtained applying this combination procedure is depicted in Fig. 14a for the time slice and Fig. 14b for the 3D seismic data cube.

For better enhancement of the internal channel media and the boundaries of the major and minor channels, the following composition was considered. The CWT spectral decomposed image of the Grubbs filter attribute for 25 Hz, the CWT-instantaneous amplitude attribute for 35 Hz and the CWT-energy attribute for 45 Hz attribute were selected as the red, the green and the blue components, respectively. The 2D RGB combined representation and the 3D representation of these components are depicted in Fig. 14c and d, respectively. As it could be seen, the minor branches are well predicted and the boundary of the major branch has been clearly identified in both its parts. In the next combination procedure for a better detection of the channel's boundary, a combination of the CWT-GLCM variance attribute for 25 Hz single frequency as the red, the CWT-Prewitt for 35 Hz single frequency as the green and the CWT-semblance for 45 Hz single frequency as the blue components were selected. The result of this combination for time slice are shown in Fig. 15a and the 3D cube of this combined attribute is represented in Fig. 15b. The channel's boundary was clearly detected and both the major and the minor branches have been clearly identified The GLCM and the gradient curvature attributes then

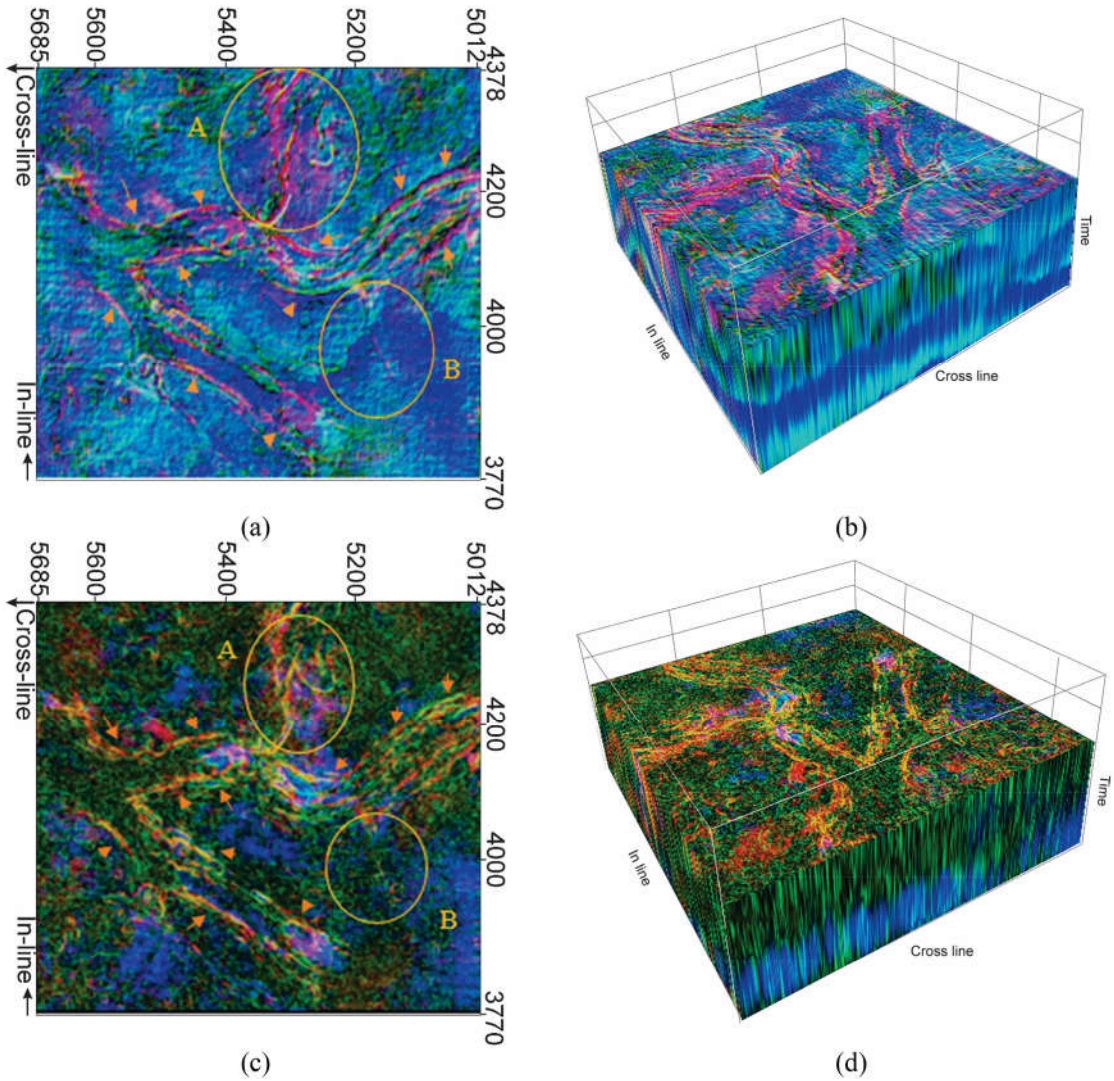

Fig. 15 Representation of the time slice with the RGB composition of the CWT-GLCM variance for 25 Hz as the red, CWT-Prewitt 35 Hz as the green and CWT- semblance 45 Hz as the blue. **b** The 3D RGB composition with the same components as in (**a**). **c** Representation of the time slice with the RGB composition of the CWT-GLCM variance for 25 Hz as the red, CWT-curvature gradient for 35 Hz as the green and CWT-energy for 45 Hz as the blue. **d** The 3D RGB composition with the same components as in (**c**)

combined to enhance the channel system in the seismic image. To build the next RGB image, the 25 Hz CWT-GLCM variance, the 35 Hz CWT-curvature and the 45 Hz CWT-energy are selected as the red, the blue and the green components, respectively. The results obtained for 2D and 3D illustration are presented in Fig. 15c and d, respectively. These results were promising for detection of channel's boundary. Both the minor and the major boundaries were detected by the new RGB attribute composition. The next combination strategy was to use advantage of the boundary detection related attributes and anomaly detection in the channel filling sediments, which are the curvature gradient, the Prewitt filter and the instantaneous amplitude attributes. Therefore, the RGB composition was performed subsequently by selecting the CWT-curvature gradient for 25 Hz as the red, the CWP-Prewitt filter for 35 Hz as green and the CWT-instantaneous amplitude for 45 Hz as the blue components. Result of applying this composition on time slice is depicted in Fig. 16a, and for the 3D seismic data in Fig. 16b. As it could be seen, the channel's boundary is clearly detected and variation in filling sediments is obvious by change in color through the inner parts of the major channel branches. Finally, to integrate the advantages of all attribute combinations depicted in this section for enhancing the boundary and the inner texture of the channel simultaneously, the CWT decomposed spectrum of the GLCM variance attribute for 25 Hz, the CWT-RMS amplitude attribute for 35 Hz and

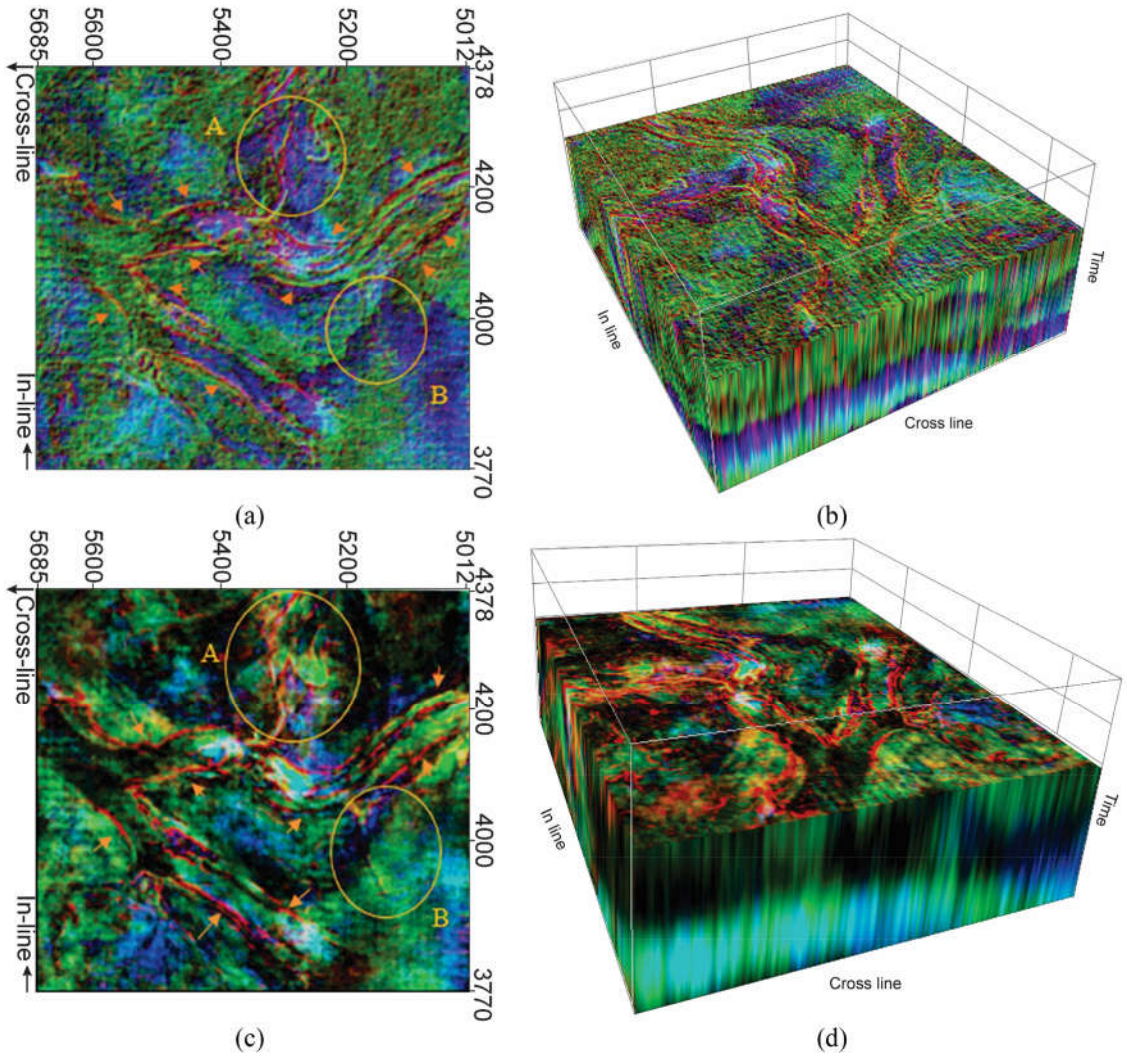

Fig. 16 Representation of the time slice with the RGB composition of the CWT-curvature gradient for 25 Hz as the red, CWT-Prewitt for 35 Hz as the green and CWT-instantaneous amplitude for 45 Hz as the blue components. **b** The 3D RGB composition with the same components as in (**a**). **c** Representation of the time slice with the RGB composition of the CWT-GLCM variance for 25 Hz as the red, CWT-RMS amplitude for 35 Hz as the green and CWT-energy for 45 Hz as the blue components. **d** The 3D RGB composition with the same components as in (**c**)

the CWT-energy attribute for 45 Hz were considered as the red, the green and the blue components, respectively.

The two-dimensional image and the three-dimensional cube of this RGB combination are presented in Figs. 16c and d. The obtained results enhance the channel boundary, while the internal properties of the channel system are also well separated from the surrounding media. Figure 16d, exhibits the three-dimensional representation of this RGB attribute, precisely detected the minor branch, which was not previously identified by any other previous single or combined attributes. The final composed RGB cube illustrates that a precis delineation of the channel system in 3D seismic data could be achieved through a practical combination of the seismic attributes and to use advantages of any single attribute to extract related information.

Conclusion

The obtained results of applying the proposed strategy for the identification of a buried channel have shown that the multi-seismic attribute combination provides images for geological interpretation better than the single attribute. Although the previous studies have used a combination of two attributes, the strategy herein used is a stepwise integration of useful information coming from various attributes,

in order to find the best possible solution for a specific problem in identification of the seismic properties of the buried channel. Some attributes identify the channel's border, while other attributes separate the channel system based on the difference in seismic properties of sediment inside and outside the channels. The strategy here proposed is based on the use of one attribute in order to identify each one of these individual properties through the RGB combination method. The investigation on different 2D and 3D combination of different seismic attributes on the CWT decomposed images has shown that the use of the CWT-GLCM for 25 Hz section, of the CWT-RMS for 35 Hz section and the CWT-energy for 45 Hz section show the seismic properties of the channel system. The obtained results have shown that if these attributes were extracted on a spectral decomposed section by the CWT method, they will exhibit a better image. The extraction of a specific attribute on a selected single frequency section was the better solution to obtain the most informative combined image. The investigation on different 2D and 3D combination of different attributes on the CWT decomposed images has shown that the use of the CWT-GLCM for 25 Hz section, the CWT-RMS for 35 Hz section and the CWT-energy for 45 Hz section show the seismic properties of the channel system.

References

Alaei N, Roshandel Kahoo A, Kamkar Rouhani A, Soleimani M (2018) Seismic resolution enhancement using scale transform in the time-frequency domain. Geophysics 83:V305–V314. https://doi.org/10.1190/geo2017-0248.1

AlShuaibi AA, Khalaf FI (2011) Development and lithogenesis of the palustrine and calcrete deposits of the Dibdibba Alluvial Fan, Kuwait. J Asian Earth Sci 42(3):423–439. https://doi.org/10.1016/j.jseaes.2011.05.014

Amin A, Deriche MA (2015a) Hybrid approach for salt dome detection in 2D and 3D seismic data. IEEE Int Conf Image Process 27–30:2537–2541. https://doi.org/10.1109/ICIP.2015.7351260

Amin A, Deriche M (2015b) A new approach for salt dome detection using a 3D multidirectional edge detector. Appl Geophys 12:334–342. https://doi.org/10.1007/s11770-015-0512-2

Amin A, Deriche M (2016) Salt-dome detection using a codebook-based learning model. IEEE Geosci Remote Sens Lett 13:1636–1640. https://doi.org/10.1109/LGRS.2016.2599435

Anees A, Shi W, Ashraf U, Xu Q (2019) Channel identification using 3D seismic attributes and well logging in lower Shihezi formation of Hangjinqi area, northern Ordos Basin, China. J Appl Geophys 163:139–150. https://doi.org/10.1016/j.jappgeo.2019.02.015

Anyiam UO, Uzuegbu E (2020) 3D seismic attribute-assisted stratigraphic framework and depositional setting characterization of frontier Miocene to Pliocene aged Agbada formation reservoirs, deep offshore Niger Delta Basin. Mar Pet Geol 122:104636. https://doi.org/10.1016/j.marpetgeo.2020.104636

Atashbari V, Tingay M, Amrouch K (2018) Stratigraphy, tectonics and hydrocarbon habitat of the Abadan plain basin: a geological review of a prolific middle eastern hydrocarbon province. Geosciences 8(12):496. https://doi.org/10.3390/geosciences8120496

Auguy C, Calvès G, Calderon Y, Brusset S (2017) Seismic evidence of gas hydrates, multiple BSRs and fluid flow offshore Tumbes Basin, Peru. Mar Geophys Res 38:409–423. https://doi.org/10.1007/s11001-017-9319-2

Barnes AE (2016) Handbook of poststack seismic attributes. Society of Exploration Geophysicists, Tulsa

Berthelot A, Solberg AHS, Morisbak E, Gelius L-J (2011) Salt diapirs without well defined boundaries—a feasibility study of semi-automatic detection. Geophys Prosp 59:682–696. https://doi.org/10.1111/j.1365-2478.2011.00950.x

Berthelot A, Solberg AHS, Gelius LJ (2013) Texture attributes for detection of salt. J Appl Geophys 88:52–69. https://doi.org/10.1016/j.jappgeo.2012.09.006

Bitrus PR, Iacopini D, Bond CE (2016) Defining the 3D geometry of thin shale units in the Sleipner reservoir using seismic attributes. Mar Pet Geol 78:405–425. https://doi.org/10.1016/j.marpetgeo.2016.09.020

Boashash B (2015) Time-frequency signal analysis and processing: a comprehensive reference. Academic Press, Elsevier Publications, Amsterdam

Bourget J, Ainsworth RB, Thompson S (2014) Seismic stratigraphy and geomorphology of a tide or wave dominated shelf-edge delta (NW Australia): process-based classification from 3D seismic attributes and implications for the prediction of deep-water sands. Mar Pet Geol 57:359–384. https://doi.org/10.1016/j.marpetgeo.2014.05.021

Boustani B, Javaherian A, Nabi-Bidhendi M, Torabi S, Amindavar HR (2019) Mapping channel edges in seismic data using curvelet transform and morphological filter. J Appl Geopys 160:57–68. https://doi.org/10.1016/j.jappgeo.2018.11.004

Bulat J, Long D (2001) Images of the seabed in the Faroe-Shetland channel from commercial 3D seismic data. Mar Geophys Res 22:345–367. https://doi.org/10.1023/A:1016343431386

Campbell TJ, Richards FWB, Silva RL, Wach G, Eliuk L (2015) Interpretation of the Penobscot 3D seismic volume using constrained sparse spike inversion, Sable sub-Basin, offshore Nova Scotia. Mar Pet Geol. https://doi.org/10.1016/j.marpetgeo.2015.08.009

Chopra S, Marfurt KJ (2007) Seismic attributes for prospect identification and reservoir characterization. Soc Explor Geophy. https://doi.org/10.1190/1.9781560801900.fm

Civile D, Lodolo E, Alp H, Ben-Avraham Z, Cova A, Baradello L, Accettella D, Burca M, Centonze J (2014) Seismic stratigraphy and structural setting of the adventure plateau (Sicily Channel). Mar Geophys Res 35:37–53. https://doi.org/10.1007/s11001-013-9205-5

Damuth JE, Olson HC (2001) Neogene-quaternary contourite and related deposition on the West Shetland slope and Faeroe-Shetland channel revealed by high-resolution seismic studies. Mar Geophys Res 22:369–398. https://doi.org/10.1023/A:1016395515456

Farfour M, Yoon WJ, Kim J (2015) Seismic attributes and acoustic impedance inversion in interpretation of complex hydrocarbon reservoirs. J Appl Geophys 114:68–80. https://doi.org/10.1016/j.jappgeo.2015.01.008

Farrokhnia F, Kahoo AR, Soleimani M (2018) Automatic salt dome detection in seismic data by combination of attribute analysis on CRS images and IGU map delineation. J Appl Geophys 159:395–407. https://doi.org/10.1016/j.jappgeo.2018.09.018

Halpert AD, Clapp RG, Biondi B (2014) Salt delineation via interpreter-guided 3D seismic image segmentation. Interpretation 2:T79–T88. https://doi.org/10.1190/INT-2013-0159.1

Hsiung K-H, Su C-C, Yu H-S, Chang J-H (2015) Morphology, seismic characteristics and development of the sediment dispersal system along the Taiwan-Luzon convergent margin. Mar Geophys Res 36:293–308. https://doi.org/10.1007/s11001-015-9251-2

Hui G, Li S, Guo L, Somerville ID, Wang P, Wang Q (2018) Mechanisms of submarine canyon formation on the northern continental

slope of the South China Sea. Geol J 54(6):3389–3403. https://doi.org/10.1002/gj.3346

Iacopini D, Butler RWH, Purves S, McArdle N, De Freslon N (2016) Exploring the seismic expression of fault zones in 3D seismic volumes. J Struct Geol 89:54–73. https://doi.org/10.1016/j.jsg.2016.05.005

Kolla V, Posamentier HW, Wood LJ (2007) Deep-water and fluvial sinuous channels—characteristics, similarities and dissimilarities, and modes of formation. Mar Pet Geol 24:388–405. https://doi.org/10.1016/j.marpetgeo.2007.01.007

Li X, Chen Q, Wu C, Liu H, Fang Y (2016) Application of multi-seismic attributes analysis in the study of distributary channels. Mar Pet Geol 75:192–202. https://doi.org/10.1016/j.marpetgeo.2016.04.016

Li W, Yue D, Colombera L, Du Y, Zhang S, Liu R, Wang W (2021) Quantitative prediction of fluvial sandbodies by combining seismic attributes of neighboring zones. J Petrol Sci Eng 196:107749. https://doi.org/10.1016/j.petrol.2020.107749

Lomask J, Clapp RG, Biondi B (2007) Application of image segmentation to tracking 3D salt boundaries. Geophysics 72:P47–P56. https://doi.org/10.1190/1.2732553

Mirkamali MS, Keshavarz FKN, Bakhtiari MR (2016) Evolution analysis of miocene channels and faults in offshore area of strait of Hormuz (Eastern part of Persian Gulf) using seismic meta-attributes. J Pet Sci Eng 147:116–128. https://doi.org/10.1016/j.petrol.2016.05.012

Nikoo A, Roshandel Kahoo A, Hassanpour H, Saadatnia H (2016) Using a time-frequency distribution to identify buried channels in reflection seismic data. Digit Signal Process 54:54–63. https://doi.org/10.1016/j.dsp.2016.03.008

Radad M, Gholami A, Siahkoohi HR (2015) S-transform with maximum energy concentration: application to non-stationary seismic deconvolution. J Appl Geophys 118:155–166. https://doi.org/10.1016/j.jappgeo.2015.04.010

Radfar A, Chakdel AR, Nejati A, Soleimani M, Taati F (2019) New insights into the structure of the South Caspian Basin from seismic reflection data, Gorgan Plain, Iran. Int J Earth Sci 108:379–402. https://doi.org/10.1007/s00531-018-1659-x

Raef AE, Meek TN, Totten MW (2016) Applications of 3D seismic attribute analysis in hydrocarbon prospect identification and evaluation: Verification and validation based on fluvial palaeochannel cross-sectional geometry and sinuosity, Ness County, Kansas, USA. Mar Pet Geol 73:21–35. https://doi.org/10.1016/j.marpetgeo.2016.02.023

Shafiq MA, Wang Z, AlRegib G, Amin A, Deriche M (2017) A texture-based interpretation workflow with application to delineating salt domes. Interpretation 5:SJ1–SJ19. https://doi.org/10.1190/INT-2016-0043.1

Shahbazi A, Soleimani M, Thiruchelvam V, Ka Fei T, Babasafari AA (2020) Integration of knowledge-based seismic inversion and sedimentological investigations for heterogeneous reservoir. J Asian Earth Sci 202:104541. https://doi.org/10.1016/j.jseaes.2020.104541

Soleimani M (2013) Simulation of petroleum exploration based on a conceptual decision model: taking the Dezful embayment in southwestern Iran as an example. Pet Explor Dev 40:476–480. https://doi.org/10.1016/S1876-3804(13)60060-9

Soleimani M (2015) Seismic imaging of mud volcano boundary in the east of Caspian sea by common diffraction surface stack method. Arab J Geosci 8:3943–3958. https://doi.org/10.1007/s12517-014-1497-5

Soleimani M, Aghajani H, Heydari-Nejad S (2018a) Salt dome boundary detection in seismic image via resolution enhancement by the improved NFG method. Acta Geod Geophys 53:463–478. https://doi.org/10.1007/s40328-018-0222-3

Soleimani M, Aghajani H, Heydari-Nejad S (2018b) Structure of giant buried mud volcanoes in the South Caspian Basin: enhanced seismic image and field gravity data by using normalized full gradient method. Interpretation 6:T861–T872. https://doi.org/10.1190/INT-2018-0009.1

Tvedt ABM, Rotevatn A, Jackson CAL (2016) Supra-salt normal fault growth during the rise and fall of a diapir: perspectives from 3D seismic reflection data, Norwegian North Sea. J Struct Geol 91:1–26. https://doi.org/10.1016/j.jsg.2016.08.001

Wang Z, Hegazy T, Long Z, AlRegib G (2015) Noise-robust detection and tracking of salt domes in postmigrated volumes using texture, tensors and subspace learning. Geophysics 80:WD101–WD116. https://doi.org/10.1190/geo2015-0116.1

Wang R, Wang Z, Osumanu A, Zhang G, Li B, Lu Y (2019) Grid density overlapping hierarchical algorithm for clustering of carbonate reservoir rock types: a case from Mishrif formation of West Qurna-1 oilfield. Iraq J Petrol Sci Eng 182:106209. https://doi.org/10.1016/j.petrol.2019.106209

Wu X (2016) Methods to compute salt likelihoods and extract salt boundaries from 3D seismic images. Geophysics 81:IM119–IM126. https://doi.org/10.1190/GEO2016-0250.1